# Performance Analysis of Super-Orthogonal Space-Time Trellis Coded MIMO-OFDM Systems over the One-Ring Channel

by


**Kun Yang**


**Thesis in partial fulfilment of the degree of**
**Master in Technology in**
**Information and Communication Technology**


**Agder University College**
**Faculty of Engineering and Science**


**Grimstad**
**Norway**
**May 2007**

# Abstract

With the rapid development of wireless communications, the available bandwidth for wireless applications becomes more and more insufficient. Therefore, how to improve data rate without expending bandwidth becomes a main goal in modern communication system design. Recently, two wireless communication schemes, which can be used to effectively combat with multi-path fading, are widely investigated around the world. One is the multiple-input multiple-output (MIMO) technology and another is the orthogonal frequency division multiplexing (OFDM). As a result, a combined system, MIMO-OFDM, can be used for wireless communications to jointly explore the advantages of the above two strategies.

In the study of MIMO-OFDM systems, the space-time block codes (STBC) and the space-time trellis codes (STTC) are two efficient coding approaches. The former can be used to offer a full diversity gain, and the later can provide the systems with a large coding gain. Since 2003, super-orthogonal space-time trellis codes (SOSTTC), a new coding method processing the merits of both STBC and STTC, have been developed. However, whether or not it can perform just as well in a MIMO-OFDM system over a frequency-selective channel is still unknown. In addition, a communication channel plays a very important role on a communication system. A channel model is used to describe a realistic communication channel and its various model parameters are considered to influence the system performance such as symbol error rate (SER) as well as bit error rate (BER). Therefore, the effects on SER and BER, caused by changing channel parameters, are worth to be investigated.

In the thesis, a new SOSTTC scheme for 16QAM constellation which can be used for high speed wireless communications is applied to a MIMO-OFDM system. To examine the performance of the proposed MIMO-OFDM system based on SOSTTC, the one-ring MIMO channel model is studied by evaluating the effects of antenna spacing, channel profiles and maximum Doppler frequency shift.

In MATLAB simulations, the SER and the BER performance results show that enlargement of the antenna spacing can bring a higher diversity gain, and the enlargement of the antenna spacing at base station can achieve better system performance than at the mobile station. In the channel profiles, the model E can gain more 1.5dB on the SER than the other models at a SER of $10^{-2}$. In addition, the larger maximum Doppler frequency shift can cause more data errors by assuming non-perfect channel state information (CSI). Finally, by using SOSTTC, the system performance on SER can be improved by 0.5 to 1dB at a SER of $5 \times 10^{-4}$, comparing it with the STBC in the same MIMO-OFDM system.

According to the above results, it will be more efficient to increase antenna spacing at

the base station and it is necessary to adjust the coding scheme and signal power to avoid performance decrease in a different communication environment and at a different speed of the mobile unite. Moreover, the SOSTTC can be integrated with MIMO-OFDM system to increase system performance.

*Keywords*: MIMO-OFDM, SOSTTC, 16QAM, One-ring MIMO channel model, SER, BER.

# Acknowledgment

This thesis is the final part of the two-year Masters program in Information Communication Technology (ICT) at Agder University College (AUC) and has been carried out from January to May 2007 by myself independently. The total credits for the master thesis is equal to 30 ECTS.

I would like to acknowledge all those who offered help to me during my work. First of all, I gratefully thank Dr. Yi Wu, My Supervisor at Agder University College for his continued support and supervision in my project. Thanks are also due to Prof. Matthias Pätzold for his useful suggestions and guidance. I would also like to express sincere thanks to Mrs. Katharina Pätzold for her help on using Latex. Finally I would like to thank Mr. Stein Bergsmark and Mrs. Sissel Andreassen for their coordination of our studies and daily life in Grimstad.

Kun Yang

*Grimstad, May 2007.*

# Contents

# List of Tables

# List of Figures

# Chapter 1

# Introduction

## 1.1 Background

Recently, mobile communication has begun to permeate every aspect of our daily lives. However, with the development of mobile communications, the frequency spectrum becomes more and more crowed. As a result, the quest for high data rates with a high spectral efficiency is considered to be the main trend in the evolution of mobile communication systems.

To achieve this goal, new concepts and methods are introduced. Multiple antenna systems, often called multi-input multi-output , were proven to be an efficient method to increase the channel capacity and system performance dramatically in [1]. The basic idea was to implement multi-antennas in both transmitters and receivers. Nevertheless, in high data rate communication, the wireless channel becomes frequency selective. As a result, the intersymbol interference (ISI) can cause tremendous influence on the system performance. To reduce the ISI, a modulation method, called orthogonal frequency division multiplexing, which increases the symbol duration by dividing the entire channel into many narrow sub-channels, is combined with MIMO.

In the MIMO-OFDM systems, the space-time block codes employing the multi-antennas can offer full antenna diversity gain, which was introduced by Alamouti in [2]. Afterwards, trellis codes introduced by Ungerboeck in [3] have been combined with STBC by Siwamogsatham and Fiz in [4]. In their paper, the state transitions of the encoder trellis diagram were designed by applying Ungerboeck's rules [3] and the transmission matrix in each state employed Alamouti's scheme [2]. It was defined that the minimum distance between the transmission matrices is larger then zero. As a result, the data rate was limited by the size of the orthogonal matrices set. This problem has been resolved by utilizing several orthogonal sets in [5][6]. Additionally, Jafarkhani and Seshadri [7] developed the principle further and referred to it as "super-orthogonal space-time codes". After that, Corneliu [8] extended it to quadrature amplitude modulation (QAM) for MIMO wireless links.

## 1.2 Problem Statement

The aim of the master's thesis is to evaluate the performance of advanced MIMO-OFDM systems in a frequency-selective fading channel. In particular, the influence of various channel parameters will be considered, such as the maximum Doppler frequency shift, the channel profile, the antenna spacings at the transmitter and the receiver side, on the performance of super-orthogonal space-time trellis coded MIMO-OFDM systems. Novel signal designs and optimization methods for MIMO-OFDM systems may also be studied. The investigation will be based on computer simulation. The results are supposed to lead to several publications.

In order to solve the main problem, the main problem has been divided into three sub-problems.

*How to implement the MIMO-OFDM system?*
Because all the tests and analyses are done in the system, realizing the MIMO-OFDM system is the highest priority. Every system is built based on a specific communication standard. Research and development without standard will not be admitted by the other researchers. A communication standard defines how a data frame is composed, how many sub-carriers exist in the system, what kind of modulation can be used, which data rate can be achieved and so on. Therefore, which standard will be used is important.

According to the standards, I can define the basic structure of the system, which includes the coding, modulation, channels, decoding, demodulation, antenna diversity and so on. In each part, there are a lot of algorithms and models which can be found in academic papers. Hence, to understand and compare them is another question.

Some criterions, which can be used to judge the correctness of my program, are needed. Some classical papers can be used for this purpose. How to choose the criterions and use the useful result to check my work is a problem too.

*How to implement the Super-Orthogonal Space-Time Codes in my system?*
Super-Orthogonal Space-Time Codes are considered as the most difficult part of the whole project. To achieve the maximum coding gain, the signal constellation should be partitioned sophisticatedly. How to divide the signal constellation will influence the efficiency of the whole system. What's more, because of the particular structure of the coding scheme, the Viterbi decoding algorithm is consider as a reasonable candidate. However, because of

the limitation of our computer hardware, the whole process may be very time-consuming. In order to save time, implementing the decoding part with C and making an interface between C and MATLAB will be an option for my work.

*How to implement the one-ring frequency-selective channel and choose the channel parameters?*
Nowadays the data rate in mobile communication systems becomes higher and higher. For the each symbol, the channel varies very fast. As a result, the channel becomes frequency selective for the high data rate mobile communications. There are many channel parameter computing methods proposed by different researchers. Different channel suits for different environments. Therefore, How to choose them for the one-ring model is a problem. Before implementing the channel model in the system, the correctness of channel should be guaranteed. Normally this is done by comparing statistical properties with the results in the relative papers. Yet which properties can be used for criterions is worth to be considered. In addition, there are a lot of channel parameters which may influence the channel properties, how to choose them and how to set their values is also important. The implementation of channel estimation is also considered to be significant in the realistic communication system. Therefore, it will be included in the sub-problem.

## 1.3 Delimitations

The research is limited to the physical layer of mobile communication, which means the subject areas such as protocols, medium access techniques, Qos and applications will be ignored. Because recently the quadrature amplitude modulation (QAM) is one of the most popular modulation schemes, the constellations in the super-orthogonal space-time trellis will be limited in 16QAM.

Some of my work is based on previous research done by the mobile communication group of AUC. The candidates of frequency-selective channel which I am going to implement have been proposed by prof. Matthias Pätzold. Some theoretical work on Super-Orthogonal Space-Time codes has been done by PhD. Yi Wu.

All the tests and simulations are limited to the computers. The practical environment tests and electronic circuit design are not included in the project.

## 1.4 Importance Of The Project

This project involving one of the most popular systems and a very advanced coding scheme can be a very attractive solution for mobile communications. If a good result can be obtained, it may be employed by big communication vendors and offer some improved theoretical results for the future work.

Furthermore, the mobile communication group in AUC has developed some channel models and signal constellation design. The communication link in the project can be a useful platform to test the statistical properties of channel models and the new coding techniques, which can offer some experimental results to modify or prove the new techniques.

In addition, as far as we know, the SOSTTC has been implemented in the MIMO system over a flat channel [8]. However, in high data rate communication systems, the channels are usually frequency-selective. Therefore, it's worthwhile to evaluate its performance in the popular MIMO-OFDM systems over a frequency-selective channel. What's more, the effect of antenna spacings and channel profiles in the channel model, which decides the diversity gain and the frequency correlation function, is still unknown in the Super-Orthogonal Space-Time Trellis Coded MIMO-OFDM system. In addition, the influence on a channel estimation algorithm caused by Maximum Doppler Shift is worth to be investigated.

## 1.5 Thesis Overview

The remainder of this paper is organized as follows:

**Chapter 2** introduces the principle of space-time codes such as space-time block codes, space-time trellis codes and super-orthogonal space-time Trellis codes. In addition, the overview of MIMO-OFDM system is also included. The one-ring frequency-selective channel model and its parameter computing methods are described as well.

**Chapter 3** proposes the structure of the super-orthogonal space-time Trellis Coded MIMO-OFDM system and describes how to implement its every part in detail.

**Chapter 4** presents theoretical reasons why choose theses channel parameters for evaluation and how to test them in the system. The corresponding results and discussions are also given in each section.

**Chapter 5** draws conclusions from the results and proposes some ideas for future work

# Chapter 2

# Theory And State-of-the-Art

## 2.1 Space-Time Codes

### 2.1.1 Space-Time Block Codes

The well-known space-time block codes, which were proposed by Alamouti in 1998 [2], are considered to be a simple but smart transmit diversity design in multi-antenna systems. The early transmit diversity technique , called delay diversity scheme [9], is to transmit the same symbol from both antennas in different symbol duration, which can make the two-path channel independently. This approach can achieve second-order diversity at the receiver with the cost of increased symbol interference and detector complexity.

However, in [2], two data streams are transmitted from the two antennas at the same symbol duration. And the structure of the transmission matrix is shown as follows:

$$\boldsymbol{M} = \begin{pmatrix} s_n^{(1)} & s_n^{(2)} \\ s_{n+1}^{(1)} & s_{n+1}^{(2)} \end{pmatrix} . \tag{2.1}$$

$$s_{n+1}^{(1)} = -s_n^{(2)H} \tag{2.2}$$

$$s_{n+1}^{(2)} = s_n^{(1)H} \tag{2.3}$$

where (1) and (2) are the index of antennas, and $n$ is the index of the symbol period. The $(\cdot)^H$ means the complex conjugate operator.

The above matrix shows that the inner product of the two columns is zero, which means the data sequences from two antennas are orthogonal. The inner product can be expressed by using:

$$s_n^{(1)} s_n^{(2)H} - s_n^{(2)H} s_n^{(1)} = 0 . \tag{2.4}$$

The diagram of the STBC is shown in figure 2.1. At the receiver side, the maximum like-

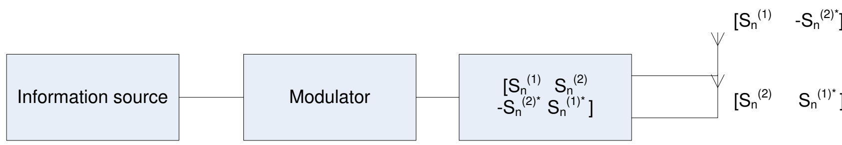


Figure 2.1: A block diagram of the STBC encoder.

lihood decoding algorithm, which assumes perfect channel state information, is employed. By assuming one receiver antenna, the received signals can be expressed by using:

$$r_1 = h_1 s_n^{(1)} + h_2 s_n^{(2)} + n_1 \tag{2.5}$$
$$r_2 = -h_1 s_n^{(2)H} + h_2 s_n^{(1)H} + n_2 \tag{2.6}$$

where $r_1$ and $r_2$ are the received signals at symbol duration 1 and 2, respectively, and $n_1$ and $n_2$ are independent gaussian noise with zero mean and unit variance. $h_1$ and $h_2$ represent the channel transfer function from antenna 1 and antenna 2, respectively and are assumed to be constant across two consecutive symbol durations, which can be given by:

$$h_1(t) = h_1(t+T) \tag{2.7}$$
$$h_2(t) = h_2(t+T) \tag{2.8}$$

where $T$ is the symbol duration. The received signals are combined as follows:

$$\tilde{s_n^{(1)}} = h_1^* r_1 + h_2 r_2^* = (\alpha_1^2 + \alpha_2^2) s_n^{(1)} + h_1^* n_1 + h_2 n_2^* \tag{2.9}$$
$$\tilde{s_n^{(2)}} = h_2^* r_1^* - h_1 r_2^* = (\alpha_1^2 + \alpha_2^2) s_n^{(2)} - h_1 n_2^* + h_2^* n_1 \tag{2.10}$$

By using the notation $d^2(x,y) = (x-y)(x^*-y^*) = |x-y|^2$, the decision rule can be expressed as follows:

$$(\alpha_1^2 + \alpha_2^2 - 1)|s_n^{(i)}|^2 + d^2(s_n^{(i)}, \tilde{s_n^{(j)}}) \leq (\alpha_1^2 + \alpha_2^2 - 1)|s_n^{(k)}|^2 + d^2(s_n^{(k)}, \tilde{s_n^{(j)}}), \forall i \neq k \tag{2.11}$$

From the above equations, it can be found that the transmission matrix can offer full diversity gain without bandwidth expansion. At the receiver side, the maximum likelihood detector can be implemented with low complexity. From the simulation result in figure 2.2, the STBC can offer 24 dB increase on the performance of BER by using two receiver antennas in the Rayleigh flat channel [2][10]. In addition, there is no need to redesign the existing systems to integrate this scheme. Therefore, it is a really intelligent design.

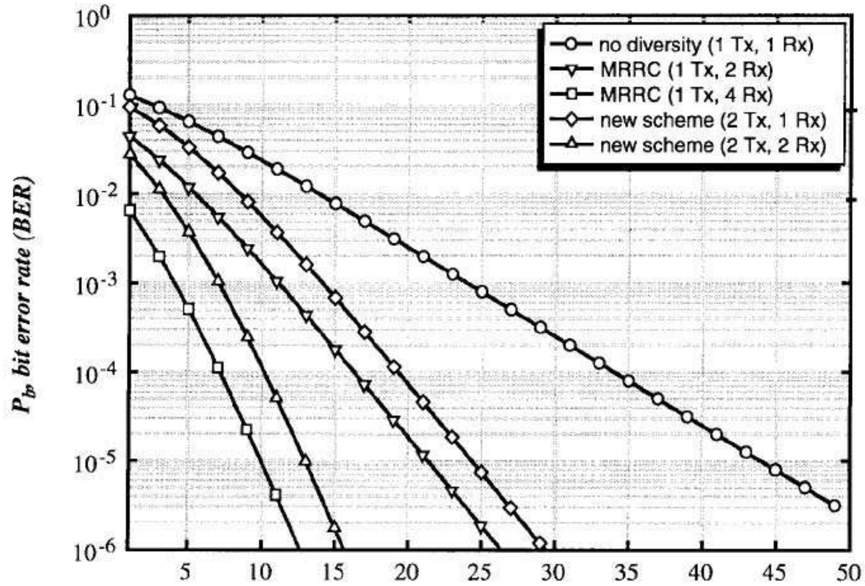


Figure 2.2: The BER performance of coherent BPSK with MRRC and two-branch transmit diversity in Rayleigh fading.

### 2.1.2 Space-Time Trellis Codes

The space-time block codes mentioned in the last section is considered to be able to provide maximum diversity gain. However, it can not achieve maximum code gain as well as full rate transmission in the limited bandwidth [11]. Therefore, an effective coding scheme, called space-time trellis codes, was firstly proposed by Tarokh [11] and it could offer a higher coding gain than STBC without loss of the diversity gain.

The matrix constructed from pairs of distinct code sequences is denoted by $\mathbf{B}$. The [11] tells us that the minimum rank among these matrices quantifies the diversity gain, while the minimum determinant of these matrices quantifies the coding gain, which is explained in appendix A. Therefore, there are two basic designs for slow Rayleigh STTC: *the rank criterion* and *the determinant criterion*. The first one aims at maximizing the minimum rank of matrix $\mathbf{B}$ over all pairs of different code words. The second one purposes to maximize the minimum determinant of the matrix $\mathbf{A}$ over all pairs of distinct code words without increasing the minimum rank, where $\mathbf{A} = \mathbf{B}\mathbf{B}^H$.

By applying this rule, the example of 4-PSK Space-Time Trellis Codes with 8 states by using two transmit antennas is shown in the figure 2.3, where $s^{(i)} = e^{\frac{j2n\pi}{N}}$ and $n \in\ 0, 1, 2, 3$. $N$ and $i$ are the number of PSK constellations and the index of transmit antennas, respectively. According to the figure 2.3, there are four kind input bits for 4-PSK: 00, 01, 10, 11. The process is as follows: The start state is 0. If 01 are the input bits, the encoder will output 2 and 0 on antenna 1 and antenna 2, respectively, with state transition to state

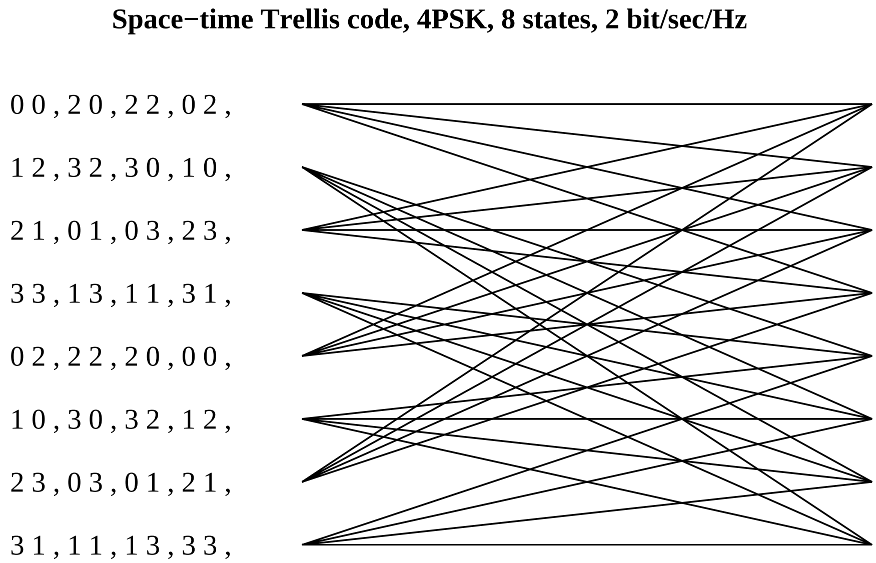


Figure 2.3: 2 transmit 4-PSK Space-Time Trellis Codes with 8 states.

1. With a current state of 1, if the input bits are 11, the encoder will output 1 and 0 on antenna 1 and antenna 2, respectively, with state transition to state 7 and so on. The trellis structure of 4PSK and 8PSK can be found in [12]. The result for 4PSK with 8 states in the Rayleigh fading channel is shown in figure 2.4. From the result, it can be found that the STTC has an excellent performance on FER, SER and BER in the Rayleigh fading channel.

### 2.1.3 Super-Orthogonal Space-Time Trellis Codes

The space-time trellis codes achieved by combining STTC and STBC has been proven to be a every effective solution on improving system performance using PSK. Nevertheless, the same partition method on the 16QAM signal constellation is still unknown. According to Ungerboeck's conclusions [3], there will be a limitation on data rate if the number of transmission matrices is not very large. Therefore, there is a kind of space-time codes, called super-orthogonal space-time trellis codes, which use an enlarged transmission matrix set and particular partition on 16QAM.

For the two transmit antennas, the transmission matrix can be expressed as follows:

$$\boldsymbol{M} = \begin{pmatrix} s_n^{(1)} & s_n^{(2)} \\ s_{n+1}^{(1)} & s_{n+1}^{(2)} \end{pmatrix} . \tag{2.12}$$

The first column is transmitted from the first antenna, while the second column is transmitted from the second antenna. In space-time codes, the two columns of the above

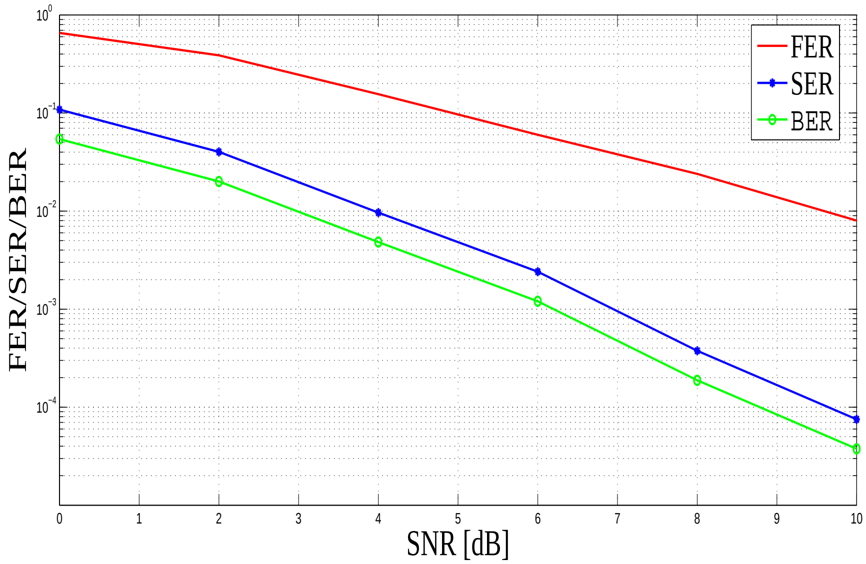


Figure 2.4: Performance of 2 transmit 4-PSK Space-Time Trellis Codes with 8 states.

transmission are orthogonal. Therefore, we get $s_n^{(2)} = e^{j\theta} s_{n+1}^{(1)H}$ and $s_{n+1}^{(2)} = -e^{j\theta} s_n^{(1)H}$, where $\theta \in \left\{0, \frac{\pi}{2}, \pi, \frac{3\pi}{2}\right\}$. There are four kinds of orthogonal transmission matrixes which can be used in our transmission instead of only the one in Alamouti's paper [2]. By applying Ungerboeck's rules [3], we know the trellis coded signal constellation should have double size compared to the uncoded one. As a result, it is necessary to use at least two orthogonal transmission matrices in the trellis codes.

The orthogonality of the above transmission matrices can guarantee the maximum diversity gain in the trellis codes. As a sequence, we only need to concentrate on the partition of the 16QAM signal constellation to achieve the maximum code gain. Here,the difference of the transmission matrices and its Hermitian transpose are defined as $\mathbf{B}$ and $\mathbf{B}^H$, respectively. According to the theory in [11], the coding gain distance $d^2$ is defined by the determinant of the matrix $\mathbf{A}$ over all different pairs of codewords $(s_n^{(1)}, s_{n+1}^{(1)})$ and $(s_n^{(2)}, s_{n+1}^{(2)})$, where $\mathbf{A} = \mathbf{B}\mathbf{B}^H$. If the $\Delta x_n$ and $\Delta y_n$ are denoted by $x_n^{(1)} - x_n^{(2)}$ and $y_n^{(1)} - y_n^{(2)}$, respectively, and $S$ can be defined as $x + jy$, the difference of transmission matrices $\mathbf{B}$ can be expressed by using

$$\mathbf{B} = \begin{pmatrix} \Delta x_n + j\Delta y_n & -\Delta x_{n+1} + \Delta j y_{n+1} \\ \Delta x_{n+1} + j\Delta y_{n+1} & \Delta x_n - j\Delta y_n \end{pmatrix} \tag{2.13}$$

The further calculation shows the coding gain can be given by

$$\begin{aligned} d^2 &= \Big[(x_n^{(1)} - x_n^{(2)})^2 + (y_n^{(1)} - y_n^{(2)})^2 \\ &\quad + (x_{n+1}^{(1)} - x_{n+1}^{(2)})^2 + (y_{n+1}^{(1)} - y_{n+1}^{(2)})\Big]^2 . \end{aligned} \tag{2.14}$$

The above equation indicates the larger code gain can be achieved if all the coordinates of the two codewords are different. It can be found that the minimum value for $d^2$ is 16 if the original 16QAM signal constellation is used. In order to obtain maximum code gain, a clever partition on the 16QAM signal constellation is proposed in [8].

Firstly, the 16QAM signal constellation is divided into four 2D subsets $A$, $B$, $C$, and

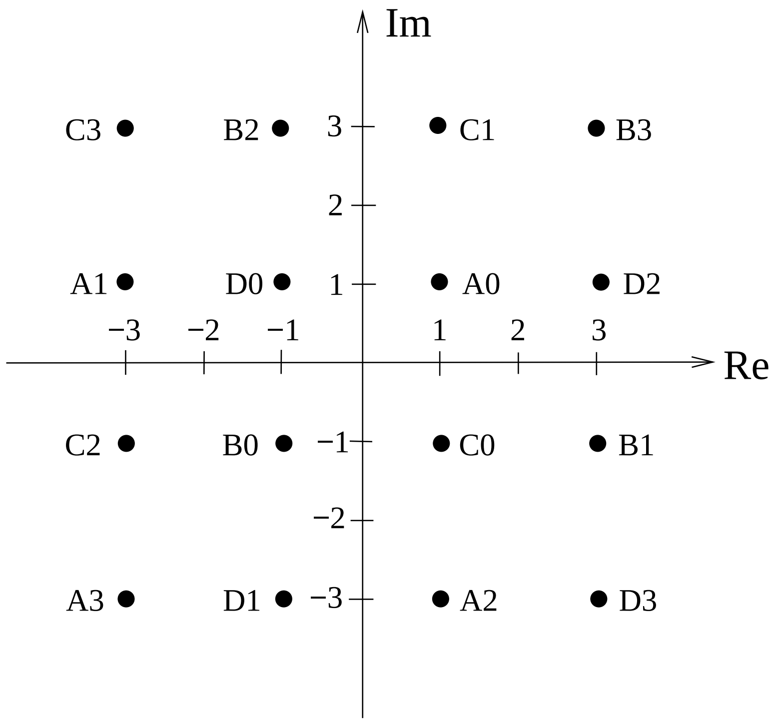


Figure 2.5: Sixteen-point 2D constellation partitioned into four subsets $(A, B, C, D)$ and into four rings $(R_0, R_1, R_2, R_3)$.

$D$ as shown in figure 2.5. As a result, the minimum-squared Euclidian distance (MSED) of each subset is four times that of the MSED of the original 16QAM signal constellation. Secondly, sixteen 4D types are formed as Cartesian product of two 2D of the above two 2D subsets, which are defined as $(A, A)$, $(A, B)$, $\ldots$, and $(D, D)$. Four sets are grouped from the 4D types , which are shown as follows:

$$SS_0 = (A, A) \cup (B, B) \cup (C, C) \cup (D, D) \tag{2.15}$$
$$SS_1 = (A, C) \cup (B, D) \cup (C, B) \cup (D, A) \tag{2.16}$$
$$SS_2 = (A, B) \cup (B, A) \cup (C, D) \cup (D, C) \tag{2.17}$$
$$SS_3 = (A, D) \cup (B, C) \cup (C, A) \cup (D, B) \tag{2.18}$$

Thirdly, the other four subsets called *rings* are formed according to the rule that there are four points of equal *norm* in each *rings* ,shown in figure 2.5. It can be found that there are four points located on the each *rings* uniformly, which means the other three points can be obtained by rotating the rest point by 90°, 180°, and 270°. Similarly, sixteen 4D types are formed as the Cartesian product of the two 2D *rings* and grouped into four subsets called *shells*, which are shown as follows:

$$SH_0 = (R_0, R_0) \cup (R_1, R_1) \cup (R_2, R_2) \cup (R_3, R_3) \tag{2.19}$$
$$SH_1 = (R_0, R_1) \cup (R_1, R_2) \cup (R_2, R_3) \cup (R_3, R_0) \tag{2.20}$$
$$SH_2 = (R_0, R_2) \cup (R_1, R_3) \cup (R_2, R_0) \cup (R_3, R_1) \tag{2.21}$$
$$SH_3 = (R_0, R_3) \cup (R_1, R_0) \cup (R_2, R_1) \cup (R_3, R_2)\,. \tag{2.22}$$

Fourthly, following [8], sixteen 4D subsets $S_m$ ($m = 0, 1, \ldots, 15$) are obtained by combining the four subsets $SS_k$ ($k = 0, 1, 2, 3$) and the four *shells* $SH_l$ ($l = 0, 1, 2, 3$), where $m = 4l + k$.

Because of the rule of the Ungerboeck [3], the trellis coded modulation should have double the size of the signal constellation, compared with the uncoded system. Therefore, it is necessary to use at least 32 4D subsets in the SOSTTC. Here, two families $F_0$ and $F_1$ are used . They use transmission matrices with parameter $\theta = 0$ and $\theta = \pi$ respectively. Finally, we select a trellis topology with 32 states and index is from 0 to 31. The subsets of the family $F_0$ are assigned to the even numbered states, while the subsets of the family $F_1$ are assigned to the odd numbered states. The 32-state trellis topology is shown as follows:

$$\begin{gathered}\{0, 2, 4, 6, 8, 10, 12, 14, 16, 18, 20, 22, 24, 26, 28, 30\} \\ \rightarrow \{0, 1, 2, 3, 4, 5, 6, 7, 8, 9, 10, 11, 12, 13, 14, 15\}\end{gathered}$$

$$\begin{gathered}\{1, 3, 5, 7, 9, 11, 13, 15, 17, 19, 21, 23, 25, 27, 29, 31\} \\ \rightarrow \{16, 17, 18, 19, 20, 21, 22, 23, 24, 25, 26, 27, 28, 29, 30, 31\}.\end{gathered}$$

The structure is demonstrate by figure 2.6. From the above figure, it is known that there are 16 possible codewords in each state. Although the sets $n$ and $n+1$, where $n \in 0, 2, 4, \ldots, 30$ have the same codeword sets, their transmission matrixes use different parameter $\theta$.

At the receiver side, it is assumed that the channel transfer functions keep constant in the duration of two consecutive symbols. The Viterbi algorithm is employed as the decoding method. A branch metric is designed to decode SOSTTC, based on the Euclidian distance. According to maximum likelihood algorithm , the branch metric $BM_n$ is given as follows:

$$BM_n = \sum_{i=0}^{1}\sum_{m=1}^{2} |r_{n+i}^{(m)} - \sum_{k=1}^{2} h_n^{(m,k)} \cdot s_{n+i}^{(k)}|^2\,. \tag{2.23}$$
$$r_n^{(1)} = h_n^{(1,1)} s_n^{(1)} + h_n^{(1,2)} s_n^{(2)} + n_1 \tag{2.24}$$
$$r_{n+1}^{(1)} = h_{n+1}^{(1,1)} s_{n+1}^{(1)} + h_{n+1}^{(1,2)} s_{(n+1)}^{(2)} + n_2 \tag{2.25}$$
$$r_n^{(2)} = h_n^{(2,1)} s_n^{(1)} + h_n^{(2,2)} s_n^{(2)} + n_3 \tag{2.26}$$
$$r_{n+1}^{(2)} = h_{n+1}^{(2,1)} s_{n+1}^{(1)} + h_{n+1}^{(2,2)} s_{(n+1)}^{(2)} + n_4 \tag{2.27}$$

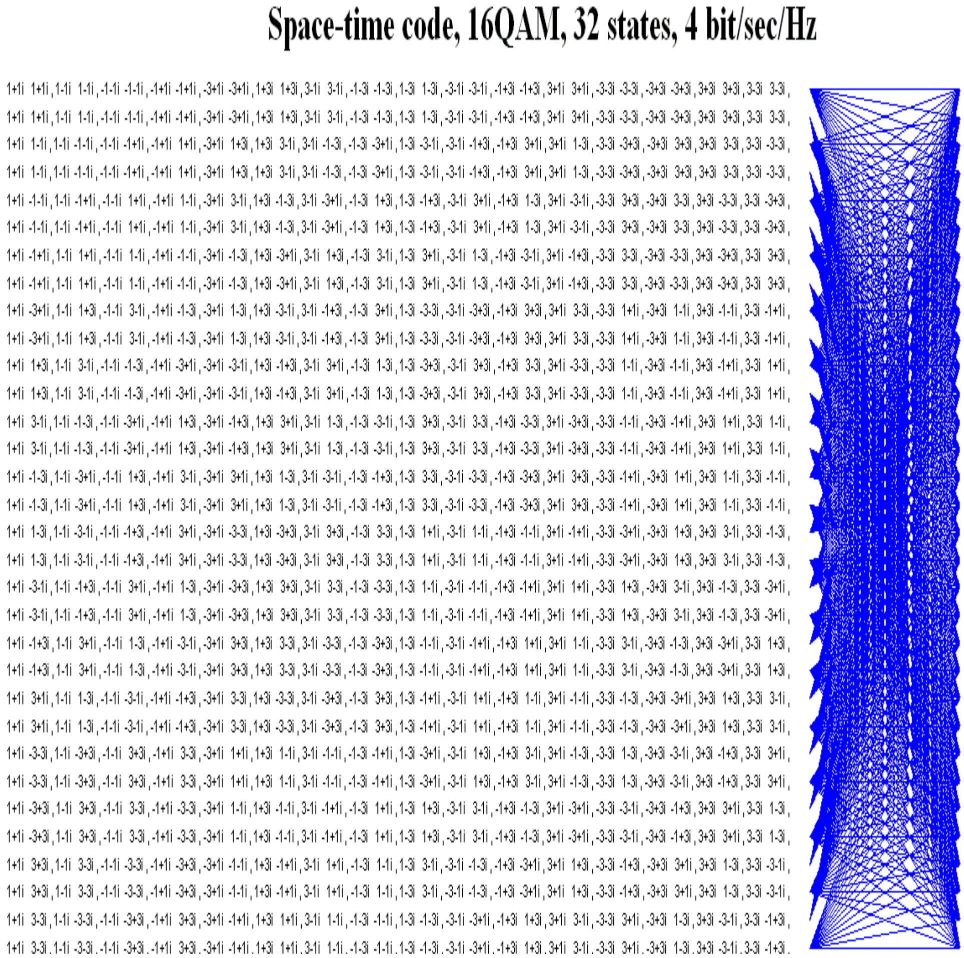


Figure 2.6: Trellis for 2 transmit Super-Orthogonal Space-Time codes on 16QAM with 32 state

In the above formulas, $m$ and $k$ are the index of receiver antennas and the index of transmitter antennas, respectively. As I mentioned before, the $h_n^{(m,k)}$ represents time-variant transfer function from $k$th transmitter antenna to $m$th receiver antenna and fulfils the condition, $h_n^{(m,k)} = h_{n+1}^{(m,k)}$. $r_{n+i}^{(m)}$ is the received signal in $m$th antenna at the $(n+i)$th symbol duration. The $n_1, n_2, n_3, n_4$ are independent Gaussian noise with zero mean and unit variance. By comparing the received matrix with the transmission ones within each of the 32 4D subsets, the closest one can be found. The survivor of each state will be recorded at each duration of symbols.

## 2.2 The MIMO-OFDM System

### 2.2.1 Orthogonal Frequency Division Multiplexing

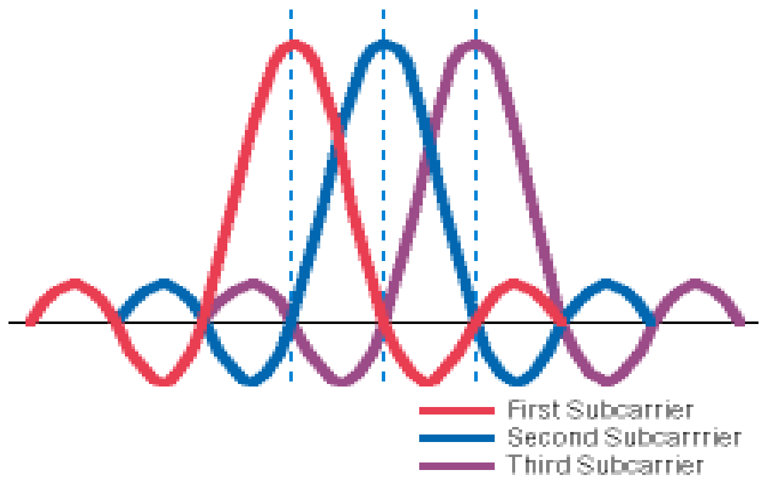


Figure 2.7: Waveform of OFDM

OFDM [13] can transmit several data streams in the same bandwidth. Each sub-carrier is orthogonal with the others [14], which can ensure the parallel data stream will not interfere with the others. It has been proven to improve the bandwidth efficiency when compared to the traditional frequency division multiplexing (FDM). In addition, it can be easily realized by Inverse Discrete Fourier Transform (IDFT),which can be expressed by using

$$X_k = \frac{1}{\sqrt{N}} \sum_{n=0}^{N-1} x_n e^{\frac{(j2\pi kn)}{N}}, 0 \leq k \leq M-1 \tag{2.28}$$

where $x_n$ is the data stream before the modulation, and $M$ is the number of sub-carriers. The waveform in time domain is demonstrated in figure 2.7.

The orthogonality guarantees that there is a null of the other carriers' spectrum at the center of each carrier's center frequency. Therefore, OFDM splits bandwidth into many narrow band channels which can be spaced very closely to each other.

After IDFT, a guard interval is inserted to combat with the ISI [15] caused by multipath delays. The guard interval, named cyclic prefix, is a copy of the last part of OFDM symbol shown in figure 2.8. Normally, the length of cyclic prefix is decided by the maximum propagation delay within the system transmission area. Because of the cyclic prefix, the influence cased by the delay echoes of previous OFDM symbols will be eliminated by discarding the cyclic prefix at the receiver side.

For the demodulation, the Discrete Fourier Transform (DFT) is used after removing

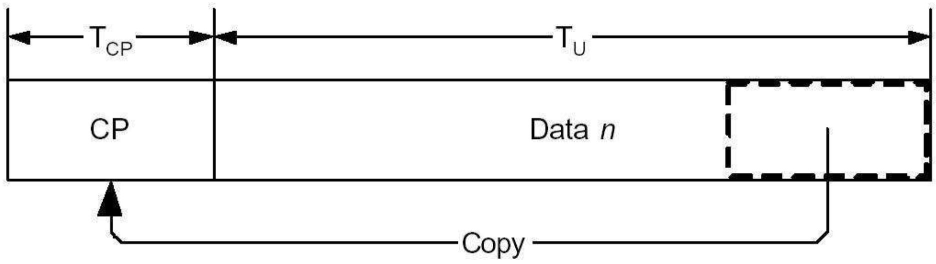


Figure 2.8: OFDM cyclic prefix

the guard interval and can be given by

$$\hat{x_k} = \frac{1}{\sqrt{N}} \sum_{n=0}^{N-1} \hat{X}_n e^{\frac{(-j2\pi kn)}{N}}, 0 \leq k \leq M-1 \tag{2.29}$$

### 2.2.2 Structure Of MIMO-OFDM System

Multiple Input Multiple Output [16][17] is a technology to employ multiple antennas on both transmitter and receiver sides to transmit radio signals. This scheme can multiplex the original serial data stream into several parallel data streams, which are transmitted from different transmitter antenna. At the receiver side, a combination of them is received. By employing the proper detector, the data streams can be separated. According to this, the data rate can be increased greatly without bandwidth expansion.

However, with the improvement of data rate, the transmitted symbol duration $T$ becomes so small that the delay spread $T_m$ can't be ignored as we did in the flat fading channel. A part of the subsequent symbol overlaps these multipath components of the previous one. As a result, more errors are caused at the receiver side. This effect is named intersymbol interference (ISI). Orthogonal frequency division multiplexing is a technology to transmit multiple data steams simultaneously by dividing the bandwidth into several orthogonal sub-carriers. MIMO with its ability to improve channel capacity is combined with OFDM [18][19], which is able to combat with ISI. The solution is considered to be a promising candidate for the fourth generation wireless system. Its basic structure is shown in figure 2.9. The original data, denoted by $X(m) = \{x(1), x(2), \ldots, x(\ell)\}$, are firstly encoded by channel encoders which can increase the signals ability to tolerate errors. Then the serial data stream $X(m)$ is transformed into several parallel streams $\{Y^{(1)}, Y^{(2)}, \ldots, Y^{(M_T)}\}$ by the MIMO encoder, where $M_T$ is the number of transmitter antennas. According to the number of OFDM subcarrier $N$, the $Y^{(p)}(n)$ is defined as $(Y^{(p)}(nN), Y^{(p)}(nN+1), \ldots, Y^{(p)}(nN+N-1)$. The data streams are modulated by OFDM and sent to the receiver through transmitter antennas.

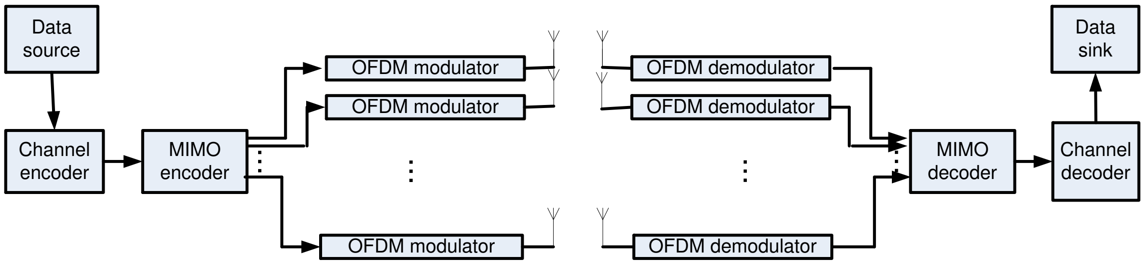


Figure 2.9: Structure of MIMO-OFDM

The received data at the receiver side is given by

$$R(m) = \begin{pmatrix} R^{(1)}(m) & R^{(1)}(m+1) & \dots & R^{(1)}(m+r) \\ R^{(2)}(m) & R^{(2)}(m+1) & \dots & R^{(2)}(m+r) \\ \dots & \dots & \dots & \dots \\ R^{(M_R)}(m) & R^{(M_R)}(m+1) & \dots & R^{(M_R)}(m+r) \end{pmatrix} \tag{2.30}$$

where $R^{(P)}(m)$ is a data vector, which fulfills $R^{(p)}(m) = (R^{(p)}(Nm), R^{(p)}(Nm+1), \dots, R^{(p)}(Nm+N-1))$. Here, $R^{(p)}(Nm+N-1)$ represents the received signal in the $p$th antenna at the $(Nm+N-1)$th symbol duration. $r$ is the number of OFDM symbol.

The time-variant channel transfer matrix in the frequency domain reads as follows:

$$H(f,t) = \begin{pmatrix} H^{(1,1)}(f,t) & H^{(1,2)}(f,t) & \dots & H^{(1,M_T)}(f,t) \\ H^{(2,1)}(f,t) & H^{(2,2)}(f,t) & \dots & H^{(2,M_T)}(f,t) \\ \dots & \dots & \dots & \dots \\ H^{(M_R,1)}(f,t) & H^{(M_R,2)}(f,t) & \dots & H^{(M_R,M_S)}(f,t) \end{pmatrix} \tag{2.31}$$

where $H^{(p,q)}(f,t)$ represents the channel transfer function of the path from the $q$th transmitter antenna to the $p$th receiver antenna and fulfils $H^{(p,q)}(f,t) = (H^{(p,q)}(f_0,t), H^{(p,q)}(f_1,t), \dots, H^{(p,q)}(f_{N-1},t))$. The relation between the transmitted data and the received data is given by using

$$R^p(m) = \sum_{q=1}^{M_T} H^{p,q}(f,m)Y^q(m) + N^p(m) \tag{2.32}$$

And note that the $N^p(m)$ is the discrete Fourier transforms of independent complex additive white Gaussian noise.

# 2.3 The Frequency-Selective Channel Model

## 2.3.1 Geometrical Model

Every channel model is limited in a specific environment whose geometrical properties play a very important role, because the geometrical approach offers methods analytically. In this project, the one-ring channel model is selected, which has been proposed in [20] and developed by Mr. Pätzold in [21]. The model is based on the following assumptions:

1. The communication link is between the base station (BS) and the mobile (MS) station which are transmitter and receiver, respectively.

2. The base station is elevated. Therefore, there is no obstruction around it. On the other hand, the mobile station is surrounded by infinite scatters located on a ring. There is no line-of-sight component between them.

3. The distance between BS and MS is much larger than the radius of the scatter ring. Two antennas are equipped on both the transmitter and receiver side.

The geometrical model is shown in the figure 2.10. The distance between the BS and the

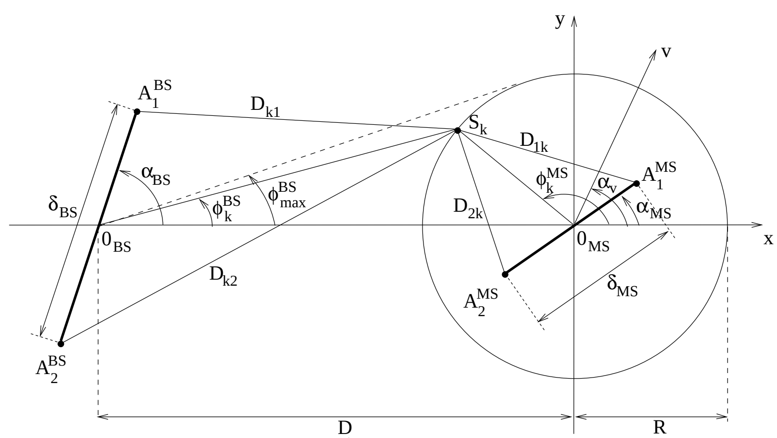


Figure 2.10: Geometrical one-ring model for a $2 \times 2$ channel

MS is defined as $D$, and $R$ denotes the ring radius. $\phi_{\max}^{\mathrm{BS}}$ is considered to be one half of the maximum angle of departure and can be expressed through $\phi_{\max}^{\mathrm{BS}} \approx \arctan(R/D) \approx R/D$. The antenna spacings $\delta_{\mathrm{BS}}$ and $\delta_{\mathrm{MS}}$ are supposed to be much smaller than $R$ and $D$. The relation can be expressed by $D \gg R \gg \max\{\delta_{\mathrm{BS}}, \delta_{\mathrm{MS}}\}$. The angles $\alpha_{\mathrm{BS}}$ and $\alpha_{\mathrm{MS}}$ define the orientation of the antenna array at BS and MS, respectively. The MS is considered to move at speed of $v$ with the motion angle $\alpha_{\mathrm{v}}$.

### 2.3.2 The Simulation Model And Its Extension To The Frequency-Selective Model

According to the above geometrical model, the time-variant complex channel gain $h^{(p,q)}(t)$, describing the link between $q$th ($q = 1, 2$) transmit antenna and $p$th ($p = 1, 2$) receiver antenna, are expressed as follows:

$$h^{(p,q)}(t) = \frac{1}{\sqrt{N}} \sum_{n=1}^{N} a_{n,q} b_{n,p} e^{\,j(2\pi f_n t + \theta_n)} \tag{2.33}$$

where

$$\begin{aligned} a_{n,q} &= e^{\,j\pi(3-2q)\frac{\delta_{\mathrm{BS}}}{\lambda}\left[\cos(\alpha_{\mathrm{BS}})+\phi^{\mathrm{BS}}_{\max}\sin(\alpha_{\mathrm{BS}})\sin(\phi^{\mathrm{MS}}_n)\right]} && (2.34)\\ b_{n,p} &= e^{\,j\pi(3-2p)\frac{\delta_{\mathrm{MS}}}{\lambda}\cos(\phi^{\mathrm{MS}}_n)-\alpha_{\mathrm{MS}}} && (2.35)\\ f_n &= f_{\max}\cos(\phi^{\mathrm{MS}}_n - \alpha_{\mathrm{V}})\,. && (2.36) \end{aligned}$$

In above equations, $N$ is referred to as the number of incoming waves. The wavelength and the maximum Doppler frequency are defined as $\lambda$ and $f_{\max}$, respectively. The phases $\theta_n$ in (2.33) are the outcomes of a random variable with a uniform distribution over $[0, 2\pi)$.

The above flat model is proposed based on the assumption that the maximum propagation delay $\tau_{\max}$ is much smaller than the duration of the data symbol $T_s$. However, for the high-data communication systems, the differences of the propagation delays are believed to be so large that it is impossible to ignore them. As a result, the channel need to be extended to be frequency-selective.

To achieve the goal, the one-ring channel model is partitioned into $\ell$ pairs of segments, as shown in figure 2.11. Each pair of segments is assigned to a propagation path. Therefore, there are $\ell$ delay paths in the model. From the figure 2.10, the maximum propagation delay can be expressed by using

$$\tau_{\max} = \frac{2R}{c_0}. \tag{2.37}$$

where $c_0$ is the speed of light. The propagation delay $\tau_n$ can be calculated as follows:

$$\begin{aligned} \tau_n &= \frac{R + \sqrt{D.^2 + R.^2 + 2DR\cos(\phi^{\mathrm{MS}}_n)} - D}{c_o} \\ &\approx \tau_{\max}\frac{1+\cos(\phi^{\mathrm{MS}}_n)}{2}. && (2.38) \end{aligned}$$

Here, the power delay profile (PDP) of model $C$ is used [22], which describes a typical large open space indoor environment. The PDP are expressed as follows:

$$s_\tau(\tau) = \sum_{l=1}^{\ell} c_l^2 \delta(\tau - \tau_l). \tag{2.39}$$

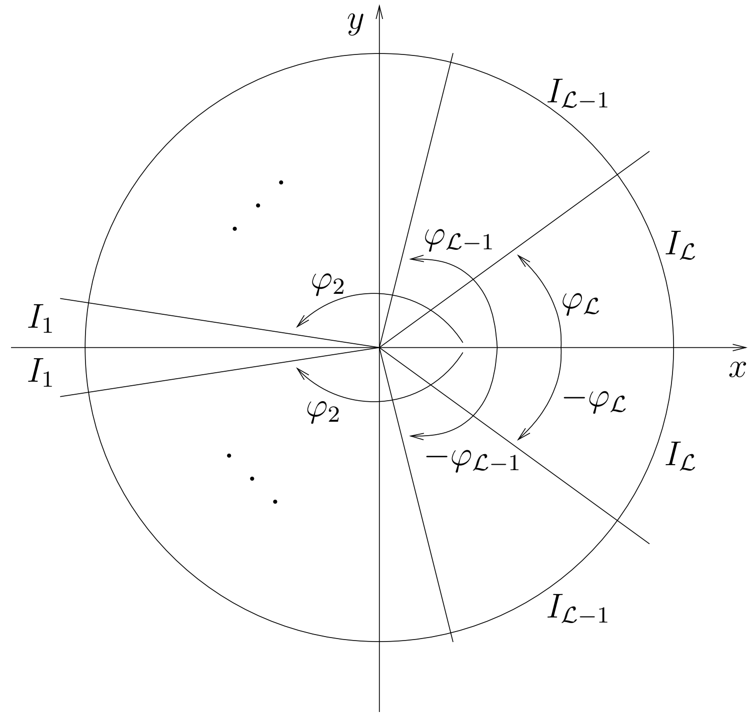


Figure 2.11: Partition of the one-ring model

The $\tau_l$ and $c_l$ are referred to as the propagation delay and attenuation factor, respectively. For all the propagation delays $\tau_n (n = 1, 2, \ldots, \ell)$, if $\tau_n$ is larger than $\tau_{l-1}$ and smaller than $\tau_l$, they are collected together and assigned to the delay $\tau_l$. The above complex channel gain $h^{(p,q)}(t)$ are developed as follows:

$$h^{(p,q)}(\tau, t) = \sum_{l=1}^{\ell} \frac{c_l}{\sqrt{N_l}} \sum_{n=1}^{N_l} a_{n,q,l} b_{n,p,l} e^{\,j(2\pi f_{n,l} t + \theta_{n,l})} \cdot \delta(\tau - \tau_l). \tag{2.40}$$

The $a_{n,q,l}$, $b_{n,p,l}$, $f_{n,l}$ and $\theta_{n,l}$ are following the definitions of $a_{n,q}$, $b_{n,p}$, $f_n$ and $\theta_n$, respectively. The Fourier transform of $h^{(p,q)}(\tau, t)$ is the time-variant transfer function $H^{(p,q)}(f, t)$,which is given by using:

$$H^{(p,q)}(f, t) = \sum_{l=1}^{\ell} \frac{c_l}{\sqrt{N_l}} \sum_{n=1}^{N_l} a_{n,q,l} b_{n,p,l} \cdot e^{\,j(2\pi f_{n,l} t + \theta_{n,l} - 2\pi f \tau_l)}. \tag{2.41}$$

The channel matrix in the system can be expressed as follows:

$$H(f, t) = \begin{pmatrix} H^{11}(f, t) & H^{12}(f, t) \\ H^{21}(f, t) & A^{22}(f, t) \end{pmatrix} \tag{2.42}$$

### 2.3.3 Parameter Computing Methods

From the above equations, it can be found that $a_{n,q,l}$, $b_{n,p,l}$, $f_{n,l}$ and $\theta_{n,l}$ are decided by the discrete angle of arrival (AOA) $\phi^{\text{MS}}$. Therefore, it is necessary to employ a parameter computing method called $\text{L}_p$-norm and generalized MEDS (GMEDS), which are explained in detail in [23] and [24][25], respectively.

By using $\text{L}_p$-norm method, the $\phi^{\text{MS}}$ can by calculated by using

$$
\begin{aligned}
E_{r_gpq} &= [\frac{1}{\tau_{max}} \int_0^{\tau_{max}} |r_gpq(\tau) - \tilde{r}_gpq(\tau)|^2].^{1/2}. && (2.43)\\
r_gpq(\tau) &= \lim_{N\to\infty} \tilde{r}_{g_{pq}}(\tau) = J_0(2\pi f_{max}\tau) && (2.44)\\
\tilde{r}_gpq(\tau) &= \frac{1}{N}\sum_{n=1}^{N} e^{\,j2\pi f_n\tau} && (2.45)
\end{aligned}
$$

where $r_gpq(\tau)$ and $\tilde{r}_gpq(\tau)$ are the temporal AutoCorrelation Function (ACF) of the reference model and the simulation model, respectively. The $f_n = f_n(\phi_n^{\text{MS}})$ is given by (2.36). The upper limit $\tau_{max}$ is given by $\frac{N}{4f_{max}}$.

By using GMEDS method, the calculation of $\phi^{\text{MS}}$ is given by

$$
\phi^{\text{MS}} = \frac{q\pi}{2N}\left(n - \frac{1}{2}\right) + \phi_0^{\text{MS}} \,, \qquad n = 1, 2, \ldots, N; q = 4 \tag{2.46}
$$

The value of $q$ decides that the scatters located uniformly on the ring. For the maximum performance, the rotation angle is defined as follows :

$$
\phi_0^{\text{MS}} := \frac{\phi_n^{\text{MS}} - \phi_{n-1}^{\text{MS}}}{4} = \frac{\pi}{2N}\,. \tag{2.47}
$$

Because of the uninform distribution of the AOAs obtained by GMEDS, it will be more convenient to test the different channel profiles.

For both of the methods, If more scatters are used in the model, the channel simulator will approach the reference model closer. One the other hand, the cost will be higher as well.

### 2.3.4 Channel Estimation

In the mobile communication system, information about the channel is really important, since it can be used for decoding algorithms and equalizers. In many decoding algorithms, the perfect channel state information is assumed. However, in the real communication system, the CSI is unknown to the transmitter and receiver. Therefore, it's necessary to design some methods to obtain CSI, which are called channel estimation. The correctness and efficiency of channel estimation algorithms decide the performance of system. Normally, channels are estimated by inserting training sequences into the data sequences. However, this method has several disadvantages [26]-[28]:

*decrease the spectral efficiency*: Because the training sequences are only used for channel estimation, the information payload will decrease.

*sensitivity to noise*: In order to avoid a large reduction in spectral efficiency, the length of training sequences is kept as small as possible. Therefore, they are sensitive to noise (longer training sequences can average out noise)

*outdated estimates*: If the channel changes so fast that the channel estimates are not accurate, it will lead to decision errors.

Here, we introduce a well-known channel estimation method, called Least Squares estimation in [26][27].

The error matrix $E_k^2$ per symbol in flat channel is expressed by using

$$E_k^2 = (R_k - S_k h_k)^H (R_k - S_k h_k) \tag{2.48}$$

where $R_k$ is the $k$th symbol on the receiver side. $h_k$ represents the channel coefficient of the $k$th symbol. The Least Squares algorithm is given by

$$\hat{h_k} = (S_k^H S_k)^{-1} S_k^H R_k \tag{2.49}$$

Here, $S_k$ are the training sequences. If they are designed to be orthogonal, the above formula can be simplified to

$$\hat{h_k} = S_k^H R_k = h_k + \tilde{N}_k \tag{2.50}$$

where $N_k$ is the additive white Gaussian noise matrix and fulfils $\tilde{N}_k = S_k^H N_k$.

# Chapter 3

# Implementation For A Communication System

## 3.1 System Overview

In order to test the channel parameters, it is necessary to build a communication system. Therefore, finding a standard which can support the MIMO-OFDM system is the first step. Currently, there are several standardization bodies intended to employ MIMO-OFDM as the key technology in the physical layer of wireless communication systems like HiperLAN/2 [17][29], IEEE802.11n [30] and so on. In this project, the HiperLAN/2 is selected as the system standard. According to the HiperLAN/2, the system works in the 5GHZ band and the total data rate can reach 54Mbit/s. The sampling rate is 20MHZ and the OFDM is employed as the modulation technique whose symbol duration is equal to 64 samples ($3.2\mu s$). In addition, 800ns is used as the cyclic prefix length $T_{CP}$.

Because the super-orthogonal space-time trellis codes are employed as the channel coding and decoding part of the communication system, the structure of the system is shown in figure 3.1. There are five parts in the communication system which are listed as follows: Channel coding, OFDM modulation, Channel, OFDM demodulation and Channel decoding. Each part will be described in detail in the following sections.

## 3.2 Channel Coding

At the transmitter side, information is transmitted in the form of a bit data stream. Following the description of [8], in two consecutive 16QAM signal intervals $n$ and $n+1$, eight information bits are sent as the input of the SOSTTC encoder, denoted by $b1_n, b2_n, b3_n, b4_n$ and $b1_{n+1}, b2_{n+1}, b3_{n+1}, b4_{n+1}$, respectively. According to figure 3.2, the first four bits $b1_n, b2_n, b3_n, b4_n$ are the input of a rate 4/5 systematic convolution encoder with total

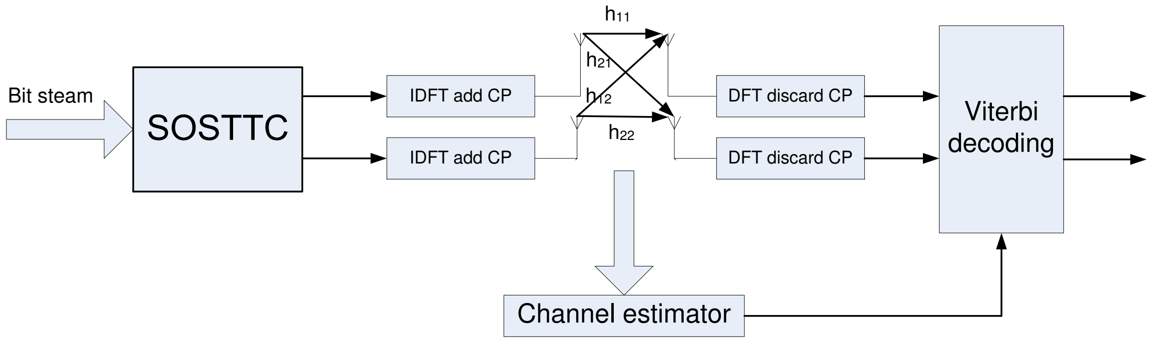


Figure 3.1: Basic structure of the communication system

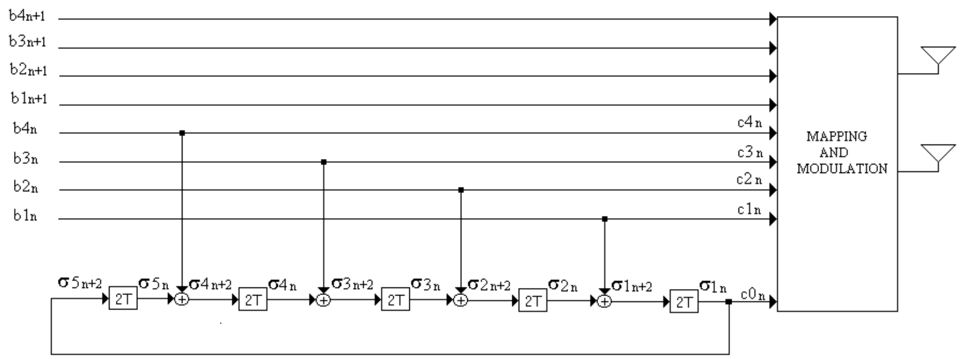


Figure 3.2: 32-state super-orthogonal space-time encoder for two transmit antennas.

memory $\nu = 5$. The five bits $c0_n, c1_n, c2_n, c3_n, c4_n$ are the output of the encoder and $di_n = \delta j_{n+2},\ j = i+1, i = 0, 1, \ldots, 4$ is obtained. The $\delta j_{n+2}$ is obtained by using:

$$\delta 5_{n+2} = \delta 1_n \tag{3.1}$$
$$\delta 4_{n+2} = \delta 5_n \oplus b4_n \tag{3.2}$$
$$\delta 3_{n+2} = \delta 4_n \oplus b3_n \tag{3.3}$$
$$\delta 2_{n+2} = \delta 3_n \oplus b2_n \tag{3.4}$$
$$\delta 1_{n+2} = \delta 2_n \oplus b1_n \tag{3.5}$$

According to the theory of SOSTTC introduced in section 2.1.3, there are 32 subsets from two families which are obtained by partitioning the 16QAM signal constellation. The first family subsets are assigned to the even-numbered states, while the second family subsets are assigned to the odd numbered states. The coded word $d0_n$ will make a choice between the family $F_0$ and $F_1$. In other words, if $d0_n$ =0, the transmission matrix with parameter $\theta = 0$ will be used, and if $d0_n = 1$, $\pi$ will be set to the parameter $\theta$. As a result, the index of the state is given by

$$p = 16d4_n + 8d3_n + 4d2_n + 2d1_n + d0_n\,. \tag{3.6}$$

which can be proved by the trellis figure shown in figure 2.6.

Table 3.1: Correspondence between $z1_u, z2_u,\ u = n$ and $n+1$, and subsets $A$, $B$, $C$, and $D$

| $z1_u z2_u$ | 2D |
|---|---|
| 0 0 | A |
| 0 1 | B |
| 1 0 | C |
| 1 1 | D |

Table 3.2: Correspondence between $z3_u, z4_u,\ u = n$ and $n+1$, and the four Rings

| $z3_u\ z4_u$ | RING |
|---|---|
| 0 0 | $R_0$ |
| 1 0 | $R_1$ |
| 0 1 | $R_2$ |
| 1 1 | $R_3$ |

Since the $d0_n$ can decide which family will be used, the bits $d1_n, d2_n, d3_n, d4_n$ can make a choice on which subsets within a family will be employed. The two bits $d1_n, d2_n$ select the 4D subsets $SS_k$ and the other two bits choose 4D subsets $SH_l$ called *shells*, where $k = 2d2_n + d1_n$ and $l = 2d4_n + d3_n$.

Up until now, the subset can be selected. The next step is to use the rest data bits $b1_{n+1}, b2_{n+1}, b3_{n+1}, b4_{n+1}$, to choose the code word within the subset. For simplicity, an easy solution is proposed in [8] based on table 3.1 and table 3.2, where the relations among $zi_n$, $di_n$ and $bi_{n+1}$ are expressed by using

$$zi_n^{(1)} = bi_{n+1},\ i = 1, \ldots, 4 \tag{3.7}$$
$$z1_{n+1}^{(1)} = d1_n \oplus z1_n^{(1)} \tag{3.8}$$
$$z2_{n+1}^{(1)} = d2_n \oplus z2_n^{(1)} \oplus (d1_n \cdot z1_n^{(1)}) \tag{3.9}$$
$$z3_{n+1}^{(1)} = d3_n \oplus z3_n^{(1)} \tag{3.10}$$
$$z4_{n+1}^{(1)} = d4_n \oplus z4_n^{(1)} \oplus (d3_n \cdot z3_n^{(1)})\,. \tag{3.11}$$

According to the tables, we can get the transmission matrix

$$\begin{pmatrix} s_n^{(1)} & s_n^{(2)} \\ s_{n+1}^{(1)} & s_{n+1}^{(2)} \end{pmatrix}.$$

where the 2D signal $s_n^{(1)}$ is selected by bits $z1_n^{(1)}, z2_n^{(1)}, z3_n^{(1)}, z4_n^{(1)}$ and 2D signal $s_{n+1}^{(1)}$ is chosen by bits $z1_{n+1}^{(1)}, z2_{n+1}^{(1)}, z3_{n+1}^{(1)}, z4_{n+1}^{(1)}$. If $d0_n = 0$, $s_n^{(2)} = s_{n+1}^{(1)*}$ and $s_{n+1}^{(2)} = -s_n^{(1)*}$.If $d0_n = 1$, $s_n^{(2)} = -s_{n+1}^{(1)*}$ and $s_{n+1}^{(2)} = s_n^{(1)*}$. Finally, two parallel orthogonal 16QAM data streams are formed from the original bit data stream.

## 3.3 OFDM Modulation

After channel coding, two orthogonal data streams are obtained. According to the principle of Space-Time codes, the orthogonality exists in the space and time domain of the same frequency domain. However, OFDM is to split the available bandwidth into several sub-channels. Therefore, the orthogonality offered by SOSTTC should be kept in each sub-channel.

According to the HiperLAN/2, there are 64 sub-channels in the bandwidth. In a OFDM symbol duration, one 16QAM symbol $s_n^{(1)}$ will be transmitted in each sub-channel. The next 16QAM symbol in the same sub-channel is supposed to be the $s_{n+1}^{(1)}$. Take 128 symbols for example, $S^{(i)}$ denotes 16QAM data vector $[s_1^{(i)}, s_2^{(i)}, \ldots, s_m^{(i)}]$, where $m = 128$ and $i = 1, 2$. Before IDFT, the $S^{(i)}$ is reshaped into two consecutive OFDM symbols, which are expressed as follows:

$$X_1^{(i)} = [s_1^{(i)}, s_3^{(i)}, \ldots, s_{2k-1}^{(i)}],\ k = 1, \ldots, 64 \tag{3.12}$$

$$X_2^{(i)} = [s_2^{(i)}, s_4^{(i)}, \ldots, s_{2k}^{(i)}],\ k = 1, \ldots, 64 \tag{3.13}$$

The length of cyclic prefix is 16 durations of 16QAM symbol. Therefore, $cp = [s_{65}^{(i)}, s_{66}^{(i)}, \ldots, s_{80}^{(i)}]$. The OFDM symbol transmission matrix is expressed as follows:

$$\begin{pmatrix} X_1^{(1)} & X_1^{(2)} \\ X_2^{(1)} & X_2^{(2)} \end{pmatrix}.$$

The whole process can be explained more clearly by the figure 3.3.

## 3.4 Channel

Until now, 64 parallel data streams will be transmitted in each antenna. It is necessary to add channel influences on the signals. Normally, the channel influences are composed of two parts: noise and channel gain . The first part are the outcomes of a random variable with a gaussian distribution $N \sim (0, 1)$, called additional white gaussian noise (AWGN). The second part is decided by formulas (2.33-2.36).

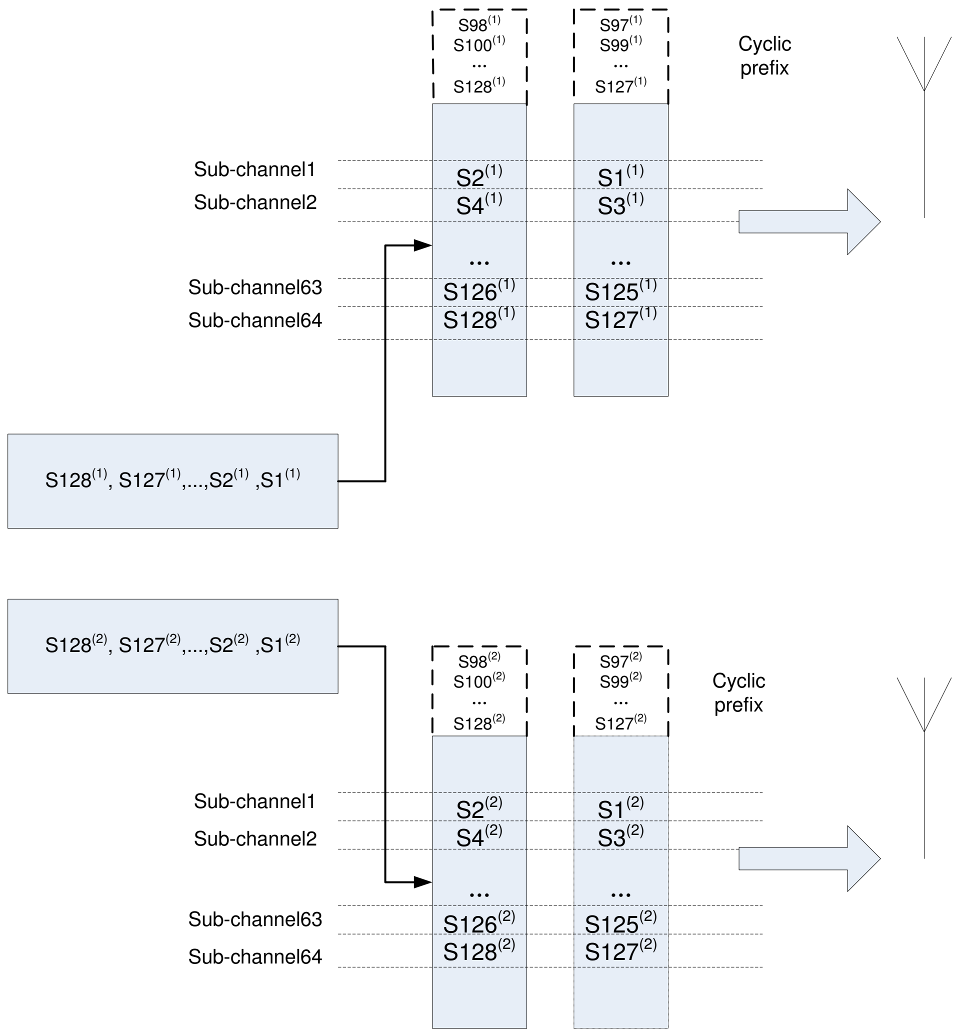


Figure 3.3: The OFDM process

In the project, the values of the parameters are shown in the table 3.3.

According to equations (2.43-2.45), 80 scatters are obtained by using $L_p$-norm with the following AOAs in table 3.4. According to the geometrical one-ring model, the delay time can be acquired by using formula (2.38). There are 80 scatters with different AOA, which result in 80 different propagation delays. If the propagation delay is within the range $[\tau_{\ell-1}, \tau_\ell]$, the corresponding scatter will be assigned to delay path $\ell$. After that, based on the formula (2.41), the channel gain can be calculated in each delay path. Here, the five indoor channel profiles used for HiperLAN/2 [22] are employed in the simulations. In these channel profiles, the time spacings of delay paths are not uniform for reducing the number of taps and the average power decreases exponentially with the increase of time. Their propagation delay profiles are shown in figure 3.4, where Model A represents a typical

| parameters | $\alpha_{\mathrm{V}}$ | $\alpha_{\mathrm{MS}}$ | $\alpha_{\mathrm{BS}}$ | $\phi_{\max}^{\mathrm{BS}}$ | N |
|---|---|---|---|---|---|
| value | 180° | 90° | 90° | 2° | 80 |

Table 3.3: Parameter values in the channel model

office environment. Model B comes from a typical large open space environment with non Line-of-sight (NLOS) conditions or an office environment with large delay spread. Model C and E correspond to typical large open space indoor and outdoor environments with large spread. Model D represents LOS conditions in a large space indoor or an outdoor environment [22].

Currently, there are two methods to add the channel gain to the signals. The first method is to do a convolution between channel gain and signals in the time domain. The second method is to multiply channel gain with signals in the frequency domain. They are expressed as follows:

$$y(t) = h(t,\tau) * S(t) + n(t) \tag{3.14}$$

$$Y(f) = H(f,\tau) \cdot S(f) + N(f) \tag{3.15}$$

where $*$ represents convolution operator.

To use the first way, it should be guaranteed that the delay interval is equal to the symbol duration. Because the time space among the delay path is not uniform, it is necesarry to transform them into a new normalized model with a delay interval of 50 $ns$, which is shown in the figure 3.5. In order to employ the second method, it should be noticed that the minimum interval of the delay path in each channel profile is 10 $ns$, compared with the sample rate 50 $ns$. Therefore, it is necessary to use $5N$-point discrete-time Fourier transform on the channel impulse response function. After that, $N$ points are chosen from the frequency response of channel. Taking Model C as an example, it can be found that most of energy focuses on the original part and the final part of the frequency response, which is shown in the figure 3.6. As a result, the first 32 frequency points and the last 32 frequency points are selected as the frequency response of the channel. This method will be employed to test the five channel profiles in the next chapter.

## 3.5 OFDM Demodulation

At the receiver side, the received signals have been influenced by the channel. After removing the guard interval from the received signals, these is no interference of the previous

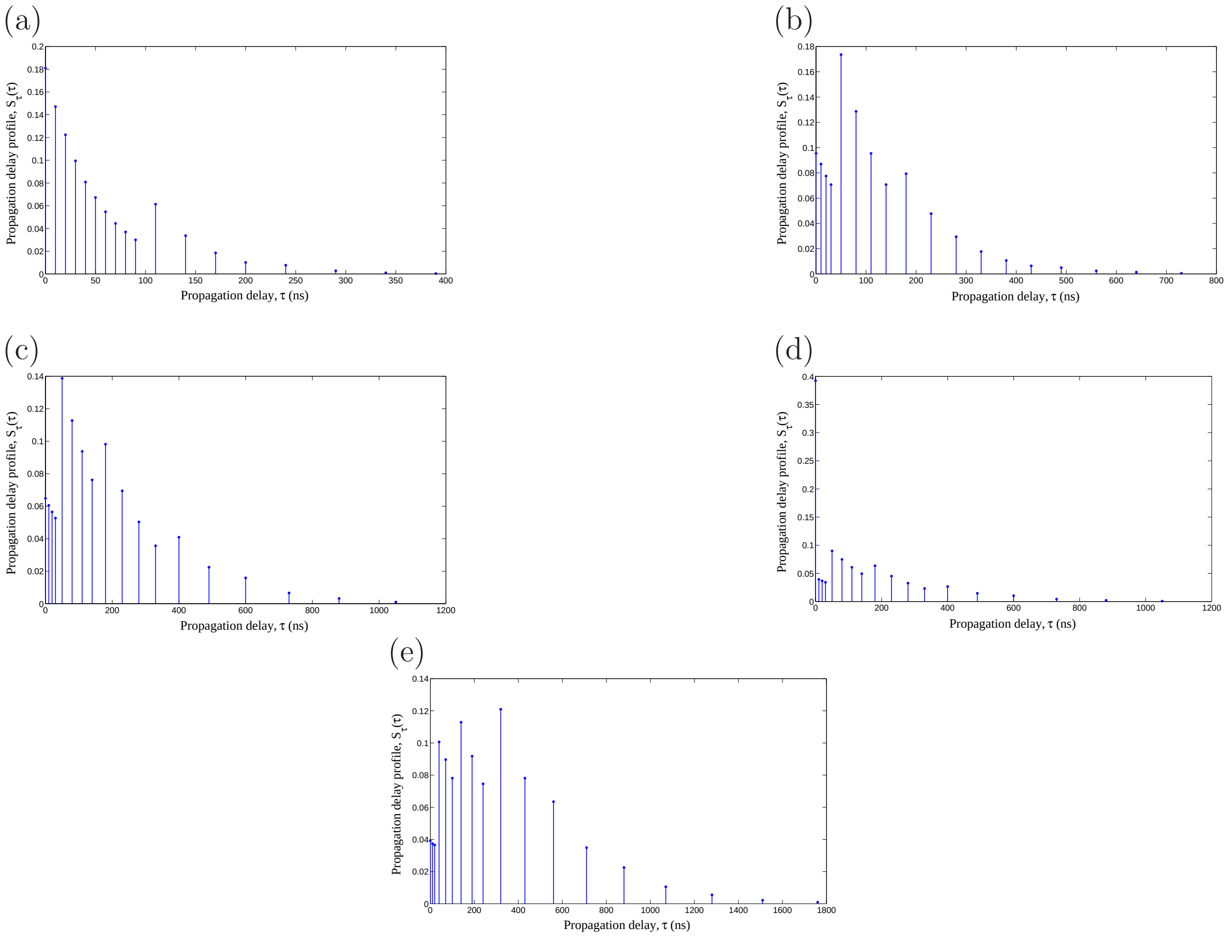


Figure 3.4: Power delay profile for: (a) Model A, (b) Model B, (c) Model C, (d) Model D and (e) Model E

OFDM symbol into the data period of the current one. Therefore, the ISI is eliminated [31]. As a sequence, a 64-channel parallel data stream from each antenna is formed. After that, 64-point FFT is performed and the parallel data are converted into serial data. The corresponding demodulation is the inverse process of the OFDM modulation.

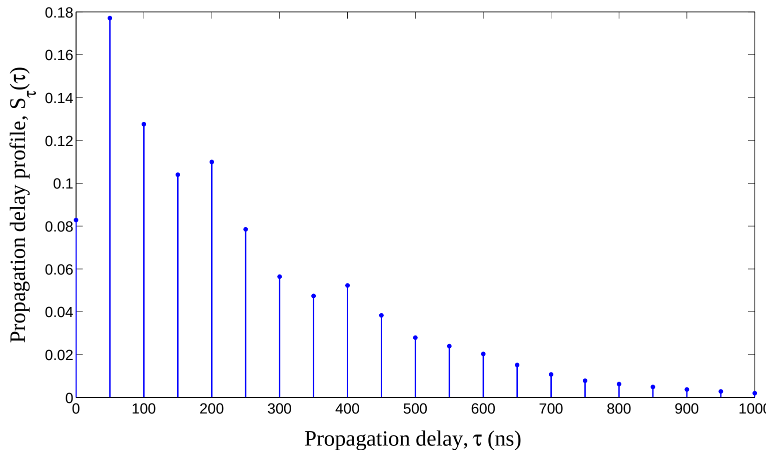


Figure 3.5: Power delay profile of normalized model C

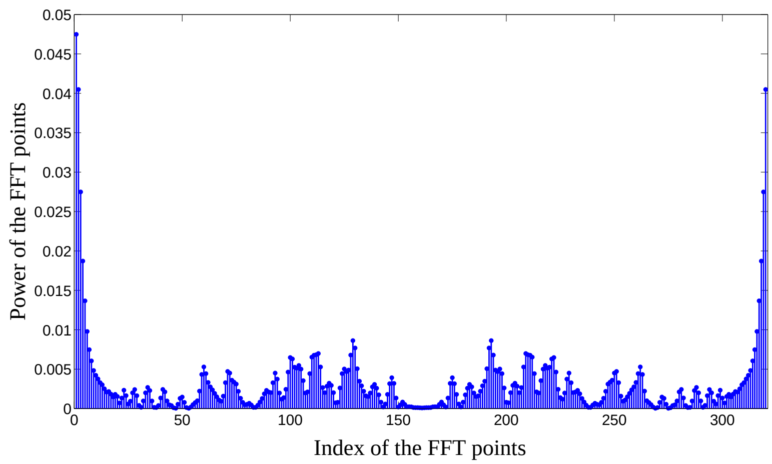


Figure 3.6: Power distribution of FFT points in model C

## 3.6 Viterbi Decoding

Currently, two parallel data streams from two receiver antennas are obtained. Based on the structure of figure 3.1, the received signals can be expressed as follows:

$$R_\gamma^{(1)} = H^{11}(f,\gamma)X_\gamma^{(1)} + H^{12}(f,\gamma)X_\gamma^{(2)} + N^1(\gamma)\,. \tag{3.16}$$

$$R_{\gamma+1}^{(1)} = H^{11}(f,\gamma+1)X_{\gamma+1}^{(1)} + H^{12}(f,\gamma+1)X_{\gamma+1}^{(2)} + N^1(\gamma+1)\,. \tag{3.17}$$

$$R_\gamma^{(2)} = H^{21}(f,\gamma)X_\gamma^{(1)} + H^{22}(f,\gamma)X_\gamma^{(2)} + N^2(\gamma)\,. \tag{3.18}$$

$$R_{\gamma+1}^{(2)} = H^{21}(f,\gamma+1)X_{\gamma+1}^{(1)} + H^{22}(f,\gamma+1)X_{\gamma+1}^{(2)} + N^2(\gamma+1)\,. \tag{3.19}$$

where $\gamma$ is the time slot of received symbol vectors and $N^1(\gamma)$,$N^1(\gamma+1)$,$N^2(\gamma)$,$N^2(\gamma+1)$ are the Fourier transforms of AWGN.

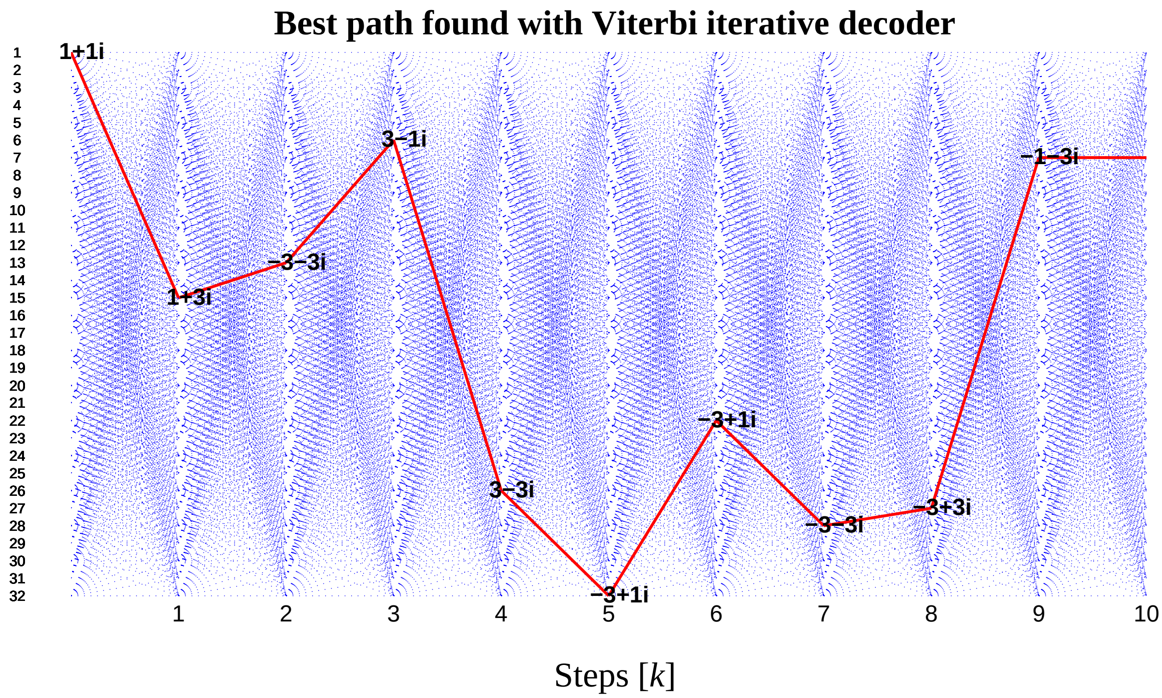


Figure 3.7: Best path by using Viterbi decoding algorithm

According to the SOSTTC principle, it is known that each subset correspond to a state. Therefore, each state has 16 codewords within the same subset. Supposing the current state is known, it can be found out the previous states which can be switched to the current state according to the trellis topology. For simplicity, the table 3.5 is used. From the table, every code word in each state can be checked by using

$$BM_n \;=\; \sum_{i=0}^{1}\sum_{m=1}^{2}|r^{m}_{n+i} - \sum_{k=1}^{2} h_n^{(m,k)} \cdot s_{n+i}^{(k)}|^2 \,. \tag{3.20}$$

As was mentioned before, the time-variant transfer functions fulfil the condition: $h_n^{(m,k)} = h_{n+1}^{(m,k)}$. For each possible previous state, the minimum branch metric is added to the previous state branch metric and recorded with the time index of the received symbols. After the OFDM symbol is finished, the path with the minimum branch metric is chosen and the data along the path is recovered as the transmitted data [32][33]. A path of the Viterbi decoding algorithm is shown in the figure 3.7.

## 3.7 Channel Estimation

In the real system, the channel state information is unknown to the receiver. In the Viterbi detector, the channel transfer function $h_n^{(m,k)}$ is necessary, according to formula (3.20). In this project, the Least Square channel estimation with special training sequences is used. In order to obtain accurate channel information, the length of a training sequence is the same as the length of a OFDM symbol. For the wideband communication, training sequences can be used in the time domain and the frequency domain. In this case, training sequences are employed in the time domain. The structure of data is shown as follows: The black

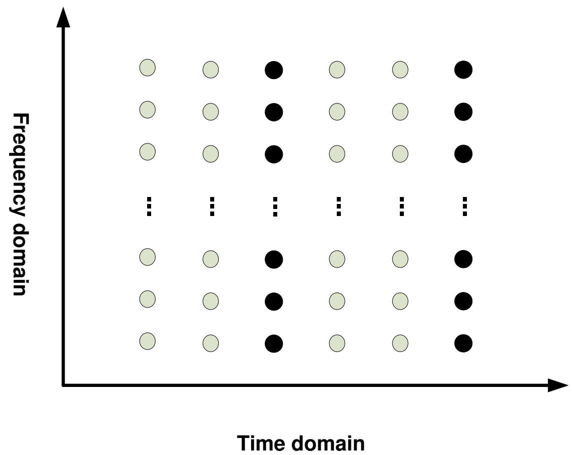


Figure 3.8: Structure of data sequences

and white points represent the training and date sequences, respectively. In order to keep the orthogonality of the space-time codes, a training sequence is inserted every two data sequences. The special training sequence is expressed as follows:

$$P(n)^{(1)} = \begin{cases} \sqrt{2}\exp^{\frac{jD_f\pi m^2}{N}} & , n = D_f m + 1,\ m = 0, 1, \ldots, M-1 \\ 0 & , \qquad\qquad others \end{cases} \tag{3.21}$$

$$P(n)^{(2)} = \begin{cases} \sqrt{2}\exp^{\frac{jD_f\pi (m+\frac{M}{2})^2}{N}} & , n = D_f m + 1,\ m = 0, 1, \ldots, M-1 \\ 0 & , \qquad\qquad others \end{cases} \tag{3.22}$$

where $N$ is the number of subcarriers. Here, $D_f = 2$ and $M$ is the number of nonzero data in a training sequence, which can be calculated by using $M = \frac{N}{D_f}$. In addition, an information matrix for channel estimation is given by

$$K = \begin{pmatrix} 1 & 1 & \ldots & 1 \\ 1 & \exp\frac{-j2\pi}{N} & \ldots & \exp\frac{-j2(N-1)\pi}{N} \\ 1 & \exp\frac{-j4\pi}{N} & \ldots & \exp\frac{-j4(N-1)\pi}{N} \\ \vdots & \vdots & \ddots & \vdots \\ 1 & \exp\frac{-j2(N-1)\pi}{N} & \ldots & \exp\frac{-j2(N-1)^2\pi}{N} \end{pmatrix} \tag{3.23}$$

We make the training sequence as a diagonal matrix $A$, shown as follows:

$$A = \begin{pmatrix} P(1) & & & \\ & P(2) & & \\ \vdots & \vdots & \ddots & \vdots \\ & & & P(N) \end{pmatrix} \tag{3.24}$$

According to the length of channel impulse $l$, the first $l$ columns are chosen from matrix $K$ to form a new matrix $F$.

$$F = \begin{pmatrix} 1 & 1 & \dots & 1 \\ 1 & \exp\frac{-j2\pi}{N} & \dots & \exp\frac{-j2l\pi}{N} \\ 1 & \exp\frac{-j4\pi}{N} & \dots & \exp\frac{-j4l\pi}{N} \\ \vdots & \vdots & \ddots & \vdots \\ 1 & \exp\frac{-j2(N-1)\pi}{N} & \dots & \exp\frac{-j2(N-1)l\pi}{N} \end{pmatrix} \tag{3.25}$$

Then the estimated channel transfer function is formed by using

$$\hat{h} = Q \cdot T^H \cdot R \tag{3.26}$$

$$T = A \cdot F \tag{3.27}$$

$$Q = (T \cdot T^H)^{-1} \tag{3.28}$$

where $R$ is the received training sequence after OFDM demodulation with discarding the guard interval.

| scatters | $\phi_n^{\text{BS}}$ | scatters | $\phi_n^{\text{BS}}$ |
|---|---|---|---|
| 1 | -3.00320709085293 | 41 | -1.95505322494554 |
| 2 | -0.83237841830576 | 42 | 1.84974232160826 |
| 3 | 0.72727255592249 | 43 | -2.06009522441790 |
| 4 | 1.38272139484274 | 44 | -2.04409629563776 |
| 5 | 1.26666121574760 | 45 | 3.01207779364855 |
| 6 | -2.52262663593284 | 46 | -0.45376873703228 |
| 7 | -0.33652260251023 | 47 | -1.06372426968473 |
| 8 | -0.45302480809319 | 48 | -1.25265532499634 |
| 9 | -0.95620840061100 | 49 | -0.82465046850049 |
| 10 | -2.26474470696926 | 50 | -0.71333515557584 |
| 11 | 1.08920327955138 | 51 | 0.55264749154306 |
| 12 | 1.20500940009395 | 52 | -2.54015655105183 |
| 13 | 1.38044676555068 | 53 | -2.98838984081165 |
| 14 | -0.14209813361519 | 54 | -0.34176583055296 |
| 15 | 0.26237767330410 | 55 | 2.27166736204453 |
| 16 | -2.52804233402189 | 56 | 2.69216547752869 |
| 17 | -0.34358141291584 | 57 | -1.54521470304572 |
| 18 | 1.31087330801838 | 58 | -2.03991075078807 |
| 19 | 2.56747932564647 | 59 | 2.28205119742899 |
| 20 | -1.45263251660963 | 60 | -1.74320298721419 |
| 21 | -0.32301221244971 | 61 | 2.82451962041915 |
| 22 | -0.33934601998289 | 62 | -0.83237841830576 |
| 23 | -0.62663272831127 | 63 | 0.97414795957226 |
| 24 | 2.54514064940172 | 64 | 2.47910421434796 |
| 25 | -1.35375006349645 | 65 | -3.20272987714997 |
| 26 | -3.22659640724209 | 66 | -2.45381070082984 |
| 27 | -2.99426563825564 | 67 | 1.84720442090746 |
| 28 | 1.21027313645929 | 68 | -0.45297420530359 |
| 29 | 0.85222547745850 | 69 | 2.47265238849207 |
| 30 | 2.78934582884663 | 70 | 1.47837157048991 |
| 31 | -1.54957482230711 | 71 | 1.20703075398936 |
| 32 | 2.18081084689481 | 72 | -1.06649617336270 |
| 33 | -1.74709405300981 | 73 | -2.21189316716542 |
| 34 | 1.77800704744472 | 74 | -2.27185554493429 |
| 35 | 2.63624452344481 | 75 | -1.88698491217412 |
| 36 | -1.66077669838419 | 76 | -0.55543353239080 |
| 37 | -1.55730928706547 | 77 | 2.08682771911275 |
| 38 | -3.18794922958075 | 78 | -0.14226218409562 |
| 39 | -2.24383837469772 | 79 | 1.84879989299026 |
| 40 | 0.84753323656091 | 80 | -0.35057308450562 |

Table 3.4: AOAs of incoming wave reflected by scatters in the channel model

| Current state | previous states | | | | | | | | | | | | | | | |
|---|---|---|---|---|---|---|---|---|---|---|---|---|---|---|---|---|
| 0 | 0 | 1 | 2 | 3 | 4 | 5 | 6 | 7 | 8 | 9 | 10 | 11 | 12 | 13 | 14 | 15 |
| 1 | 16 | 17 | 18 | 19 | 20 | 21 | 22 | 23 | 24 | 25 | 26 | 27 | 28 | 29 | 30 | 31 |
| 2 | 0 | 1 | 2 | 3 | 4 | 5 | 6 | 7 | 8 | 9 | 10 | 11 | 12 | 13 | 14 | 15 |
| 3 | 16 | 17 | 18 | 19 | 20 | 21 | 22 | 23 | 24 | 25 | 26 | 27 | 28 | 29 | 30 | 31 |
| 4 | 0 | 1 | 2 | 3 | 4 | 5 | 6 | 7 | 8 | 9 | 10 | 11 | 12 | 13 | 14 | 15 |
| 5 | 16 | 17 | 18 | 19 | 20 | 21 | 22 | 23 | 24 | 25 | 26 | 27 | 28 | 29 | 30 | 31 |
| 6 | 0 | 1 | 2 | 3 | 4 | 5 | 6 | 7 | 8 | 9 | 10 | 11 | 12 | 13 | 14 | 15 |
| 7 | 16 | 17 | 18 | 19 | 20 | 21 | 22 | 23 | 24 | 25 | 26 | 27 | 28 | 29 | 30 | 31 |
| 8 | 0 | 1 | 2 | 3 | 4 | 5 | 6 | 7 | 8 | 9 | 10 | 11 | 12 | 13 | 14 | 15 |
| 9 | 16 | 17 | 18 | 19 | 20 | 21 | 22 | 23 | 24 | 25 | 26 | 27 | 28 | 29 | 30 | 31 |
| 10 | 0 | 1 | 2 | 3 | 4 | 5 | 6 | 7 | 8 | 9 | 10 | 11 | 12 | 13 | 14 | 15 |
| 11 | 16 | 17 | 18 | 19 | 20 | 21 | 22 | 23 | 24 | 25 | 26 | 27 | 28 | 29 | 30 | 31 |
| 12 | 0 | 1 | 2 | 3 | 4 | 5 | 6 | 7 | 8 | 9 | 10 | 11 | 12 | 13 | 14 | 15 |
| 13 | 16 | 17 | 18 | 19 | 20 | 21 | 22 | 23 | 24 | 25 | 26 | 27 | 28 | 29 | 30 | 31 |
| 14 | 0 | 1 | 2 | 3 | 4 | 5 | 6 | 7 | 8 | 9 | 10 | 11 | 12 | 13 | 14 | 15 |
| 15 | 16 | 17 | 18 | 19 | 20 | 21 | 22 | 23 | 24 | 25 | 26 | 27 | 28 | 29 | 30 | 31 |
| 16 | 0 | 1 | 2 | 3 | 4 | 5 | 6 | 7 | 8 | 9 | 10 | 11 | 12 | 13 | 14 | 15 |
| 17 | 16 | 17 | 18 | 19 | 20 | 21 | 22 | 23 | 24 | 25 | 26 | 27 | 28 | 29 | 30 | 31 |
| 18 | 0 | 1 | 2 | 3 | 4 | 5 | 6 | 7 | 8 | 9 | 10 | 11 | 12 | 13 | 14 | 15 |
| 19 | 16 | 17 | 18 | 19 | 20 | 21 | 22 | 23 | 24 | 25 | 26 | 27 | 28 | 29 | 30 | 31 |
| 20 | 0 | 1 | 2 | 3 | 4 | 5 | 6 | 7 | 8 | 9 | 10 | 11 | 12 | 13 | 14 | 15 |
| 21 | 16 | 17 | 18 | 19 | 20 | 21 | 22 | 23 | 24 | 25 | 26 | 27 | 28 | 29 | 30 | 31 |
| 22 | 0 | 1 | 2 | 3 | 4 | 5 | 6 | 7 | 8 | 9 | 10 | 11 | 12 | 13 | 14 | 15 |
| 23 | 16 | 17 | 18 | 19 | 20 | 21 | 22 | 23 | 24 | 25 | 26 | 27 | 28 | 29 | 30 | 31 |
| 24 | 0 | 1 | 2 | 3 | 4 | 5 | 6 | 7 | 8 | 9 | 10 | 11 | 12 | 13 | 14 | 15 |
| 25 | 16 | 17 | 18 | 19 | 20 | 21 | 22 | 23 | 24 | 25 | 26 | 27 | 28 | 29 | 30 | 31 |
| 26 | 0 | 1 | 2 | 3 | 4 | 5 | 6 | 7 | 8 | 9 | 10 | 11 | 12 | 13 | 14 | 15 |
| 27 | 16 | 17 | 18 | 19 | 20 | 21 | 22 | 23 | 24 | 25 | 26 | 27 | 28 | 29 | 30 | 31 |
| 28 | 0 | 1 | 2 | 3 | 4 | 5 | 6 | 7 | 8 | 9 | 10 | 11 | 12 | 13 | 14 | 15 |
| 29 | 16 | 17 | 18 | 19 | 20 | 21 | 22 | 23 | 24 | 25 | 26 | 27 | 28 | 29 | 30 | 31 |
| 30 | 0 | 1 | 2 | 3 | 4 | 5 | 6 | 7 | 8 | 9 | 10 | 11 | 12 | 13 | 14 | 15 |
| 31 | 16 | 17 | 18 | 19 | 20 | 21 | 22 | 23 | 24 | 25 | 26 | 27 | 28 | 29 | 30 | 31 |

Table 3.5: States transition from the trellis topology

# Chapter 4

# Channel Parameter Evaluation And Discussions

For a MIMO channel model, the correlation properties are decided by the various channel parameters [34]. As far as I know, the channel changing speed, spatial correlation among antennas, and frequency correlation among OFDM subcarriers are corresponded to these correlation properties. Therefore, channel parameters will influence system performances including FER, BER and SER, which are worth being investigated [35]. Finally, the comparison between STBC and SOSTTC is shown. The corresponding discussions are included after the results.

## 4.1 Numerical Results With Different Antenna Spacings

Normally, the signals transmitted from different antennas elements interfere with each other. In other words, the spatial diversity gain is influenced by the signal correlation between the antenna elements. With the increase of the antenna spacing, the spatial correlation of signals will be decreased. As a result, the spatial diversity gain and the channel capacity will be improved, which will affect system performances [34][36][37].

In this case, the 2D space Cross-correlation function (CCF) of the reference model by using GMED is given by using [24]

$$\begin{aligned} CCF(\delta_{BS}, \delta_{MS}) = \; & e^{j2\pi \frac{\delta_{BS}}{\lambda}\cos(\alpha_{BS})} J_0(2\pi\{(\phi_{\max}^{BS}\delta_{BS}/\lambda)^2 \\ & \cdot \sin^2(\delta_{BS}) + 2\phi_{\max}^{BS}\delta_{BS}\delta_{MS}/\lambda^2 \\ & \cdot \sin(\alpha_{BS})\sin(\alpha_{MS}) + (\delta_{MS}/\lambda)^2\}^{1/2}). \end{aligned} \tag{4.1}$$

Its corresponding simulation model is expressed as follows:

$$C\tilde{C}F(\delta_{BS}, \delta_{MS}) = \frac{1}{N}\sum_{n=1}^{N} a_{n,1}^2(\delta_{BS}) b_{n,1}^2(\delta_{MS})\,. \tag{4.2}$$

By using formula (2.38) in the formula (4.1) and setting $\alpha_{BS} = \alpha_{MS} = \pi/2$, the reference model can be simplified as:

$$CCF(\delta_{BS}, \delta_{MS}) = J_0\left(2\pi\left(\phi_{\max}^{BS}\frac{\delta_{BS}}{\lambda} + \frac{\delta_{MS}}{\lambda}\right)\right). \tag{4.3}$$

The figures of 2D space CCF $CCF(\delta_{BS}, \delta_{MS})$ and $C\tilde{C}F(\delta_{BS}, \delta_{MS})$ are shown in the figure 4.1 and figure 4.2.

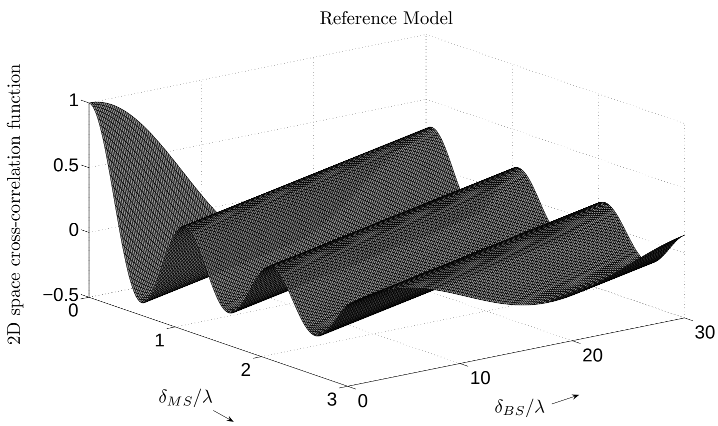


Figure 4.1: The 2D space CCF $C\tilde{C}F(\delta_{BS}, \delta_{MS})$ of the simulation model (GMEDS$_4$, $N = 80, \alpha_{BS} = \alpha_{MS} = \pi/2$, $\phi_{\max}^{BS} = 2°$).

In order to test the influence of antenna spacings, five different values for $\delta_{BS}$ and $\delta_{MS}$ are used, which are included in the table 4.1. According to the values in the table, the results

Table 4.1: Antenna spacings values

| case | 1 | 2 | 3 | 4 | 5 |
|---|---|---|---|---|---|
| $\delta_{BS}/\lambda$ | 1/2 | 1 | 30 | 30 | 1/2 |
| $\delta_{MS}/\lambda$ | 1/2 | 1 | 3 | 1/2 | 3 |

are obtained and shown in the figure 4.3.

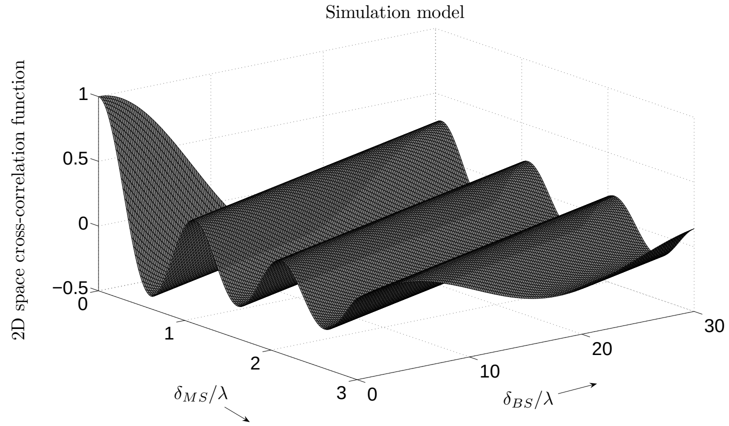


Figure 4.2: The 2D space CCF $CCF(\delta_{BS}, \delta_{MS})$ of the reference model ($N \to \infty$, $\alpha_{BS} = \alpha_{MS} = \pi/2$, $\phi_{\max}^{BS} = 2°$).

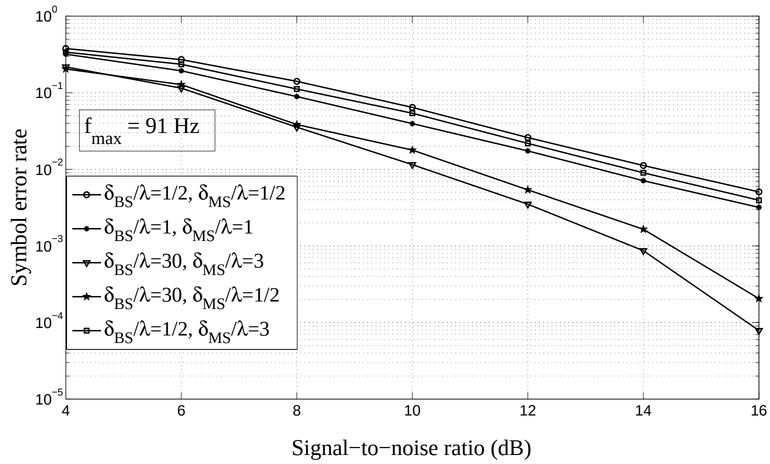


Figure 4.3: SER by using different antenna spacings.

In the simulations, the maximum Doppler frequency shift is set to $91Hz$, and the $\phi_{\max}^{BS}$ is 2°. The results show that, with the enlargement of antenna spacings at receiver side and transmitter side, the SER becomes smaller and smaller. In addition, an increasing of the BS antenna spacing achieves a higher diversity gain than the same increasing of the MS antenna spacing. Therefore, it is more efficient and convenient to enlarge the BS antenna spacing to enhance the channel capacity and system performance. The corresponding FER and BER are shown in figure 4.4 and figure 4.5. The FER is high in the frequency-selective one-ring model.

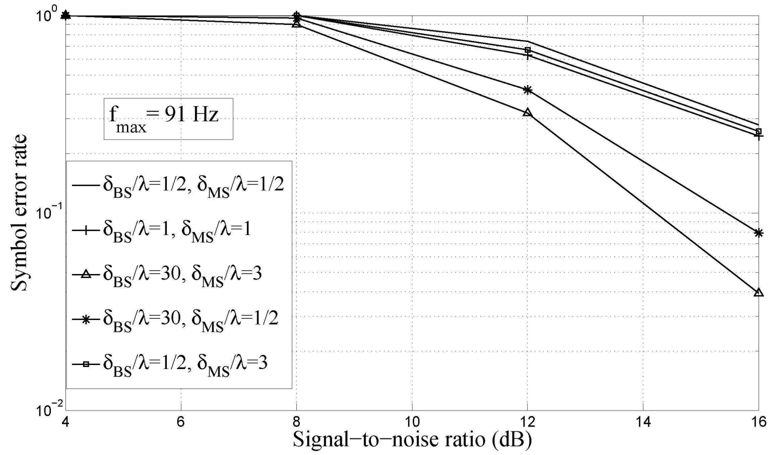


Figure 4.4: FER by using different antenna spacings.

## 4.2 Numerical Results With Different Channel Profiles

The channel profile describes the signal power distribution of the multiple delay paths in a specific environment. According to channel profile, the power delay profile can be obtained [38][39], which is defined as follows:

$$\tilde{r}_{h^{(p,q)}}(\tau, \delta t) := E\{\tilde{h}^{(p,q)}(\tau_1, t+\delta t)\tilde{h}^{(p,q)*}(\tau_2, t)\} \tag{4.4}$$

$$P_{h^{(p,q)}}(\tau) = \tilde{r}_{h^{(p,q)}}(\tau, 0) \tag{4.5}$$

where $\tilde{r}_{h^{(p,q)}}$ is the autocorrelation function (ACF) and $E\{\cdot\}$ denotes the time average operator. The power delay profile represents the average power associated with a given multiple path delay. Its average and rms delay spread are expressed as follows:

$$\mu = \frac{\int_0^\infty \tau P_{h^{(p,q)}}(\tau)d\tau}{\int_0^\infty P_{h^{(p,q)}}(\tau)d\tau} \tag{4.6}$$

$$\sigma = \sqrt{\frac{\int_0^\infty (\tau-\mu)^2 P_{h^{(p,q)}}(\tau)d\tau}{\int_0^\infty P_{h^{(p,q)}}(\tau)d\tau}} \tag{4.7}$$

The frequency correlation function (FCF) $F_{h^{(p,q)}}(f)$ is the Fourier transform of the PDP. And when $F_{h^{(p,q)}}(\delta f)$ is equal to zero, the channel response is approximately independent at frequency separations $\delta f$, which is named *coherence bandwidth*. These relationships

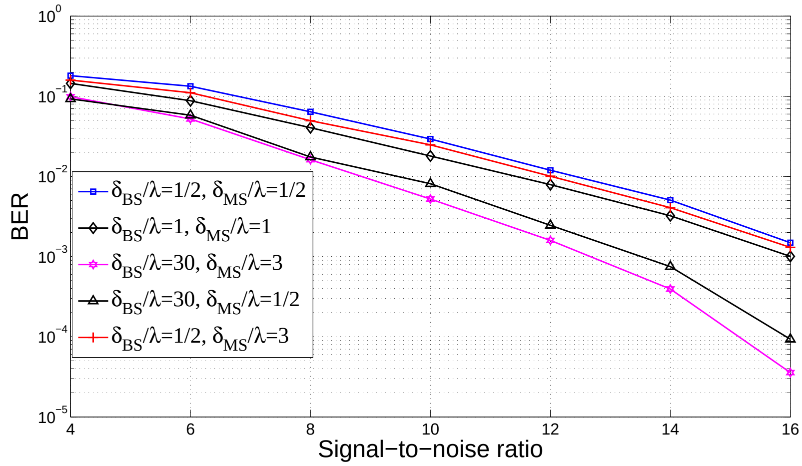


Figure 4.5: BER by using different antenna spacings.

show that different channel profiles determine different frequency correlation in a MIMO channel. As a result, the system performance can be changed.

Therefore, five different channel profiles is used whose PDP is shown in figure 3.4. In the one-ring MIMO model, the FCF is given by

$$F_{h^{(p,q)}}(f) = \sum_{l=1}^{\ell} c_l^2 \, e^{-j2\pi\tau_l f} \, . \tag{4.8}$$

According to [24], it is known that the FCF of reference model is equal to that of the simulation model. The FCF of the five channel profiles are shown in figure 4.6.

By using the above five models, the corresponding SER is obtained which is shown in figure 4.7.

The results show that model E has at least $1.5dB$ increase at a SER of $10^{-2}$, compared with the other models. This is because the frequency correlation of model E and model C changes very fast and converges to zero quickly. As a result, the correlation of subcarriers in the frequency domain is relatively smaller. Therefore, SERs of model C and model E are smaller than the ones of model A and model D.

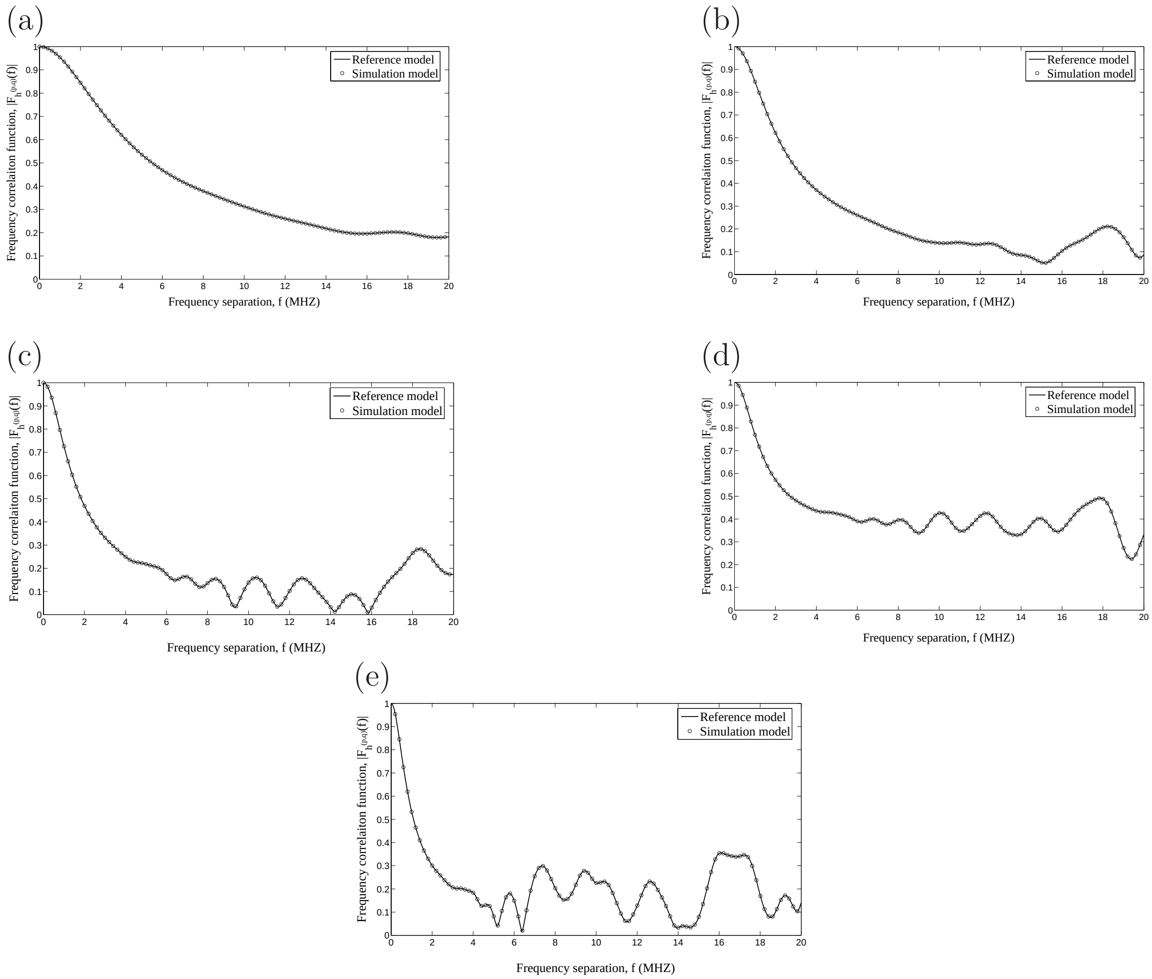


Figure 4.6: Absolute value of the FCFs $|F_{h^{(p,q)}}(f)|$ according to the 18-path HIPERLAN/2 models: (a) model A, (b) Model B, (c) Model C, (d) Model D and (e) Model E

## 4.3 Numerical Results With Different Maximum Doppler Frequency Shift

To the best of my knowledge, the channel changing speed is determined by the temporal ACF [40] which is given by

$$r_{h^{(p,q)}}(\tau): \;=\; E\{h^{(p,q)}(t+\tau)h^{(p,q)*}(t) \tag{4.9}$$

In the one-ring MIMO channel model, the ACF of the simulation model is expressed by using

$$\tilde{r}_{h^{(p,q)}}(\tau): \;=\; \frac{1}{N}\sum_{n=1}^{N} e^{j2\pi f_n \tau} \tag{4.10}$$

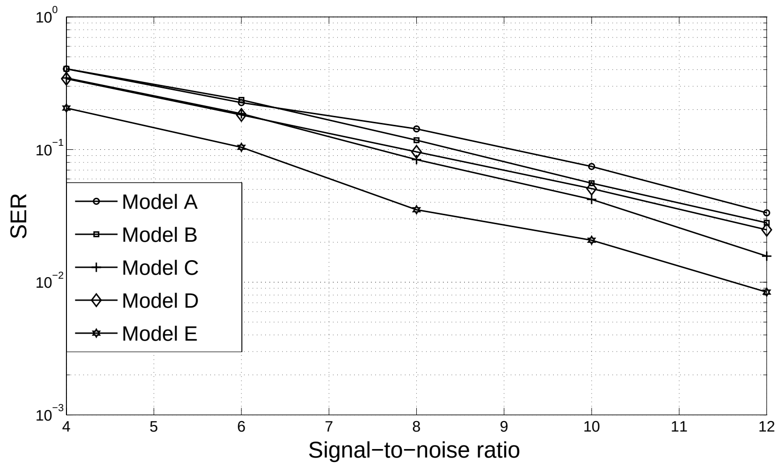


Figure 4.7: SER with different channel profiles.

where $f_n = f_n(\phi_n^{MS})$, according to formula (2.36). By increasing $N \rightarrow \infty$, the temporal ACF $\tilde{r}_{h^{(p,q)}}(\tau)$ approaches

$$\lim_{N\rightarrow\infty} \tilde{r}_{h^{(p,q)}}(\tau) = r_{h^{(p,q)}}(\tau) = J_0(2\pi f_{\max}\tau) \quad (4.11)$$

where $J_0(\cdot)$ is the zero-order Bessel function of the first kind and $r_{h^{(p,q)}}(\tau)$ is the temporal ACF of the reference model.

From the temporal ACF $r_{h^{(p,q)}}(\tau)$, it can be found that the ACF is determined by the maximum Doppler frequency. Therefore, I get the conclusion that the maximum Doppler frequency shift will influence the channel speed. However, according to the previous research, there is no influence on the system performance by changing maximum Doppler frequency with perfect CSI [41].

As was mentioned before, if the channel changes so fast that the channel estimates are not accurate, it will lead to more error bits. In other words, the maximum Doppler frequency can influence the system performance with non-perfect CSI. Here, a group of values for the maximum Doppler frequency is used, which are shown in the table 4.2. The simulation

Table 4.2: Maximum Doppler frequency shift

| case | 1 | 2 | 3 | 4 |
|---|---|---|---|---|
| maximum Doppler frequency shift(Hz) | 50 | 90 | 500 | 1000 |

results are shown in the figure 4.8.

With the increase of the maximum Doppler frequency shift, the SER of the system becomes higher and higher. The reason for it is that the channel changes faster, when the maximum Doppler frequency shift is increased. As the result, the estimated channel information is less accurate, which will lead more errors at the receiver side.

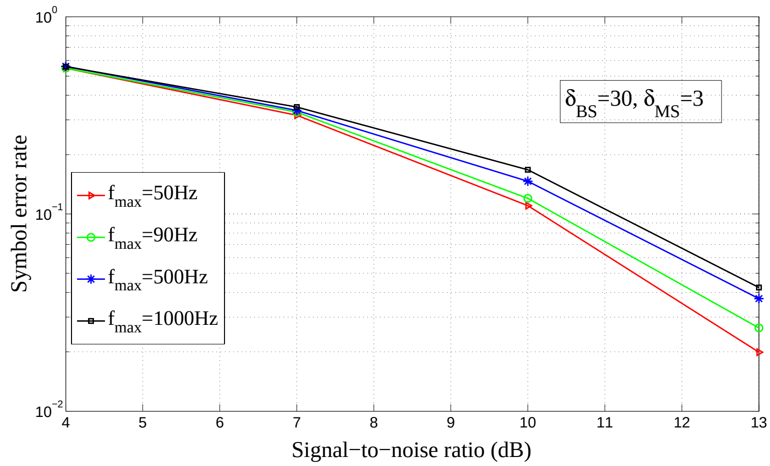


Figure 4.8: SER performance by using different maximum Doppler frequency shift.

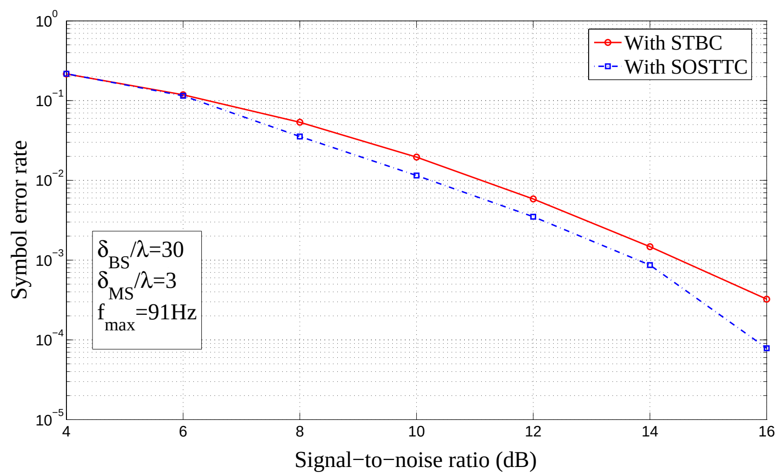


Figure 4.9: SER performance of the MIMO-OFDM system with SOSTTC and STBC.

## 4.4 Comparison Between SOSTTC And STBC

In order to illustrate the advantage of SOSTTC, the STBC and SOSTTC are implemented in the same MIMO-OFDM system. In the simulations, the $\delta_{BS}$ and $\delta_{MS}$ are 30 and 3, respectively. The maximum Doppler frequency shift is $91Hz$. The results is shown in figure 4.8.

The results show that there is a 0.5dB to 1dB increase at a SER of $5 \times 10^{-4}$ by using SOSTTC, compared with the STBC. In this case, there are 9 information bits transmitted in the two symbol duration. As a result, the SOSTTC can offer a higher coding gain than the STBC.

# Chapter 5

# Conclusions And Future work

## 5.1 Conclusions

In this thesis, the super orthogonal space-time trellis codes and the frequency-selective one-ring channel model were integrated into a MIMO-OFDM system. Based on the system, the influences on SER, FER and BER caused by different channel spatial correlation , frequency correlation and temporal correlation were evaluated. In addition, the comparison between SOTTC and STBC was done.

The chapter 2 started with principles and the state-of-the-art related to the super orthogonal space-time trellis coded MIMO-OFDM system. Particularly, the developments of space-time codes were introduced. In addition, I emphasized on the basic principle of SOSTTC and its advantages. The basic theories and structure of the MIMO-OFDM system were described as well. Finally, the principle of channel estimation in broadband communications was included.

Based on the principles in chapter 2, the SOSTTC by using 16 trellis states and 32 4D subsets were implemented in the chapter 3. After that, the data streams for OFDM modulation and demodulation were organized. Moreover, by using channel parameter computing method, the frequency-selective one-ring channel model in both time and frequency domain were implemented. In order to obtain channel state information, the Least Square channel estimation with special training sequences was employed in the system.

In order to test the relations between channel parameters and the system performance on SER, BER and FER, different values were used for antenna spacing at both base station side and mobile station side, the channel profiles and the maximum Doppler frequency shift. In order to illustrate the advantage of SOSTTC over SBTC, the comparison between them was implemented. According to the simulation results, it was known that the enlargement of antenna spacing could lead to the enhancement of system performance on SER, BER and FER and channel capacity. In addition, a increase of the BS antenna spacing caused a higher diversity gain than a increase of the MS antenna spacing. Moreover, By employing different channel profiles, it was found that the model E had a at least a 1.5db increase at a SER of $10^{-2}$, compared with the other models. The evaluation of the maximum Doppler frequency shift showed that the increase of maximum Doppler frequency shift led to outdated estimates in channel estimation with system performance decrease on SER. Finally, the comparison between the SOSTTC and the STBC in the same system revealed that the SOSTTC had a about 1dB increase at a SER of $5 \times 10^{-4}$, compared with the STBC.

## 5.2 Future Work

1.In this thesis, a method to add the channel gain in frequency domain was used. The method is to choose the 32 points and the last 32 points in frequency domain and multiply them with 64 symbols in a OFDM symbol. However, according to the simulation, It is found that for a normalized channel model, only about fifty percent energy had been added to the signal, which may cause a decrease of system performance on BER, SER and FER. In order to solve this problem, the methods for channel modelling [23], which can avoid energy loss and keep the same energy distribution, can be applied to the frequency channel gain adding method.

2.By evaluate the maximum Doppler frequency shift with channel estimation, it is found that no matter how good a channel estimation is, there will be some errors. These estimation errors will cause the decision errors at the receiver side. However, if we know the statistical properties of the errors, we can use them to reduce the decision errors. Therefore, It makes sense to model the distribution of the estimation errors and find the corresponding statistical properties.

3.Except antenna spacing, channel profiles and the maximum Doppler frequency shift, it is found that the angular spread can influence the system performance by changing the spatial correlation of the channel model [42][43]. Therefore, it is worth being investigated as well.

# Bibliography


[1] Foschini GH, and Gans MJ, "On limits of wireless communications in a fading environment when using multiple antennas," *Wireless Personal Communications*.pp. 311–335, 1998.

[2] S. M. Alamouti, "A simple transmit diversity technique for wireless communications," *IEEE J. Select. Areas Commun.*, vol. 16, no. 8, pp. 1451–1458, Oct. 1998.

[3] G. Ungerboeck, "Channel coding with multilevel/phase signals," *IEEE Trans. Inform. Theory*, vol. IT-28, pp. 56–67, Jan. 1982.

[4] S. Siwamogsatham and M. P. Fitz, "Robust space-time codes for correlated Rayleigh fading channels," *IEEE Trans. Signal Processing*, vol. 50, no. 10, pp. 2408–2416, Oct. 2002.

[5] D. M. Ionescu, K. K. Mukkavilli, Z. Yan and J. Lilleberg, "Improved 8- and 16-state space-time codes for 4 PSK with two transmit antennas," *IEEE Commun. Letters*, vol. 5, no. 7, pp. 301–303, Jul. 2003.

[6] S. Siwamogsatham and M. P. Fitz, "Improved high-rate space-time codes via orthogonality and set partitioning," in *Proc. 4th Int. Symp. on Wireless Personal Multimedia Communications, WPMC'01*, Aalborg, Denmark, Sept. 2001, vol. 1, pp. 264–270.

[7] H. Jafarkhani and N. Seshadri, "Super-orthogonal space-time trellis codes," *IEEE Trans. Inform. Theory*, vol. 49, pp. 937–950, Apr. 2003.

[8] C. E. D. Sterian, H . Singh, M. Pätzold, and B. O. Hogstad, "Super-Orthogonal Space-Time Codes with Rectangular Constellations and Two Transmit Antennas for High Data Rate Wireless Communications,", *IEEE Trans. Wireless Commun.*, vol. 5, no. 7, pp. 1857–1865, Jul. 2006.

[9] Seshadri,N., and J. Winters, "Two Signaling Schemes for Improving the Error Performance of Frequency-Division-Duplex(FDD)Transmission Systems Using Transmitter Antenna Diversity," *Int. J. Wireless Information Networks*, vol. 1, pp. 49–60, Jan. 1998

[10] A. Wittneben, "A new bandwidth efficient transmit antenna modulation diversity scheme for linear digital modulation,," *IEEE International Conf. Communications*, pp. 1630–1634, May 1993.

[11] V. Tarokh, N. Seshadri, and A. R. Calderbank, "Space-time codes for high data rate wireless communications: Performance criterion and code construction," *IEEE Trans. Inform. Theory*, vol. 44, no. 2, pp. 744–765, Mar. 1998.

[12] M. Jankiraman, *Space-Time Codes and MIMO Systems*. Boston&London:Artech House, 2004.

[13] S. Kaiser , "OFDM code-division multiplexing in fading channels," *IEEE Trans.*, vol. 50, no. 8, pp. 1266–1373, Aug. 2002.

[14] Prasad, R.,*Universal Wireless Personal Communications*. Norwood MA:Artech House, 1998.

[15] Hyunjae Kim, Hongku Kang, Wooncheol Hwang, Kiseon Kim, "A multiple guard interval based frequency error detector for OFDM systems," in *IEEE Trans.*, vol. 46,no. 2, pp. 363–367, May 2000.

[16] Ayaweera, S. K. ; Poor, H. V. , "Capacity of multiple-antenna systems with both receiver and transmitter channel state information," *IEEE Trans. Information Theory*, vol. 49, no. 10 pp. 2697–2709, Oct. 2003

[17] D. Gesbert, M. Shafi, D. S. Shiu, P. J. Smith, and A. Naguib, " From theory to practice: an overview of MIMO space-time coded wireless systems," in *IEEE J. Select. Areas Commun.* vol. 21,no. 3, pp. 281–302, 2003.

[18] Van Nee, R.,and R. Prasad, *OFDM for Wireless Multimedia Communications*. Norwood MA:Artech House, 2000.

[19] W. Y. Zou and Y. Wu, "COFDM: an overview," in *IEEE Trans. on Broadcasting,*, vol. 41,no. 1, pp. 1–8, 1995.

[20] D. S. Shiu, G. J. Foschini, M. J. Gans, and J. M. Kahn, "Fading correlation and its effect on the capacity of multielement antenna systems,," *IEEE Trans. commun.*, vol. 48,no. 3, pp. 502–513, Mar. 2000.

[21] M. Pätzold and B. O. Hogstad, "A space-time channel simulator for MIMO channels based on the geometrical one-ring scattering model," in *Proc. 60th IEEE Semiannual Veh. Technol. Conf., VTC 2004-Fall*, Los Angeles, CA, USA, Sept. 2004.

[22] J. Medbo and P. Schramm, "Channel models for HIPERLAN/2 in different indoor scenarios," ETSI EP, BRAN Meeting #3, Tech. Rep. 3ERI085B, Mar. 1998.

[23] M. Pätzold, *Mobile Fading Channels*. Chichester: John Wiley & Sons, 2002.

[24] M. Pätzold and B. O. Hogstad, "A Wideband Space-Time MIMO Channel Simulator Based on the Geometrical One-Ring Model," in *Proc. 64th IEEE Semiannual Veh. Technol. Conf., VTC 2006-Fall*, Montreal, Canada, Sept. 2006.

[25] C.-X. Wang and M. Pätzold, "Methods of generating multiple uncorrelated Rayleigh fading processes," in *Proc. 57th IEEE Semiannual Veh. Technol. Conf., VTC 2003-Spring*, Jeju, Korea, Apr. 2003, pp. 510–514.

[26] Mody,A. N. ,and G. L. Stuber, "Parameter Estimation for OFDM With Transmit Receive Diversity," in *IEEE Veh. Technol. Conf.,*, Rhodes, Greece, May 2001.

[27] Mody,A. N. ,and G. L. Stuber, "Synchronization for MIMO-OFDM Systems," in *IEEE Glo. Commun. conf.,*, San Antonio, America, Nov. 2001.

[28] Siew, J. , et al., "A Channel Estimation Method for MIMO-OFDM Systems,", in *London Communications Symposium,* London, England, Sept. 2002.

[29] ETSI, " Broadband radio access networks (BRAN); HIPERLAN Type 2; packet based convergence layer; Part 1; common part; Requirements and architectures for wireless broadband access,," Technical Report TR 101 031 V2.2.1, ETSI, Jan. 1999.

[30] IEEE, "IEEE standards for local and metropolitan area networks: integrated services (IS) LAN interface at the medium access control (MAC) and physical (PHY) layers,," Dec. 1994

[31] Lan Yang; Shixing Cheng; Haifeng Wang, " Effects of cyclic prefix on OFDM systems over time-varying channels,," in *IEEE 16th International Symposium on Personal Indoor and Mobile Radio Communications,* vol. 2,no. 11-14, pp. 750–753, Sept. 2005.

[32] Lou, H. L. , " Implementing the Viterbi algorithm,," in *IEEE Signal Processing Magazine,* vol. 12,no. 5, pp. 42–52, Sept. 1995.

[33] Man Guo; Ahmad, M. O. ; Swamy, M. N. S. ; Chunyan Wang, " An adaptive Viterbi algorithm based on strongly connected trellis decoding,," in *IEEE International Symposium on Circuits and Systems,* vol. 4,no. 5, pp. 26–29, May 2002.

[34] G. J. Byers and F. Takawira, "Spatially and temporally correlated MIMO channels: modelling and capacity analysis," *IEEE Trans. Veh. Technol.*, vol. 53, no. 3, pp. 634–643, May 2004.

[35] J. S. Sadowsky and V. Kafedziski, "On the correlation and scattering functions of the WSSUS channel for mobile communications,," *IEEE Trans. on Veh. Technol.,* vol. 47,no. 3, pp. 270–282, Feb. 1998.

[36] E. A. Jorswieck and A. Sezgin, "Impact of spatial correlation on the performance of orthogonal space-time block codes," *IEEE Commun. Letters*, vol. 8, no. 1, pp. 21–23, Jan. 2004.

[37] Baker, P. , "Spatial correlation measurements on one-hop HF radio waves,," *IEEE Trans. on Antennas and Propagation,* vol. 19,no. 6, pp. 793–794, Nov. 1971.

[38] Patzold, M. ; Szczepanski, A. ; Youssef, N. , "Methods for modeling of specified and measured multipath power-delay profiles,," *IEEE Trans. on Vehicular Technology,* vol. 51,no. 5, pp. 978–988, Sept. 2002.

[39] V. Erceg, D. G. Michelson, S. S. Ghassemzadeh, L. J. Greenstein, A. J. Rustako, Jr. , P. B. Guerlain, M. K. Dennison, R. S. Roman, D. J. Barnickel, and S. C. Wang, R. R. Miller, "MA model for the multipath delay profile of fixed wireless channels,," *IEEE J. Select. Areas Commun.,* vol. 17, pp. 399–410, Sept. 1999.

[40] Rad, H. S. ; Gazor, S. , "A cross-correlation model for non-isotropic scattering with non-omnidirectional antennas in MIMO propagation channels ,," *IEEE 6th Workshop on Signal Proc.,* pp. 251–255, Jun. 2005.

[41] H. Zhang, D. Yuan, M. Pätzold and V. D. Nguyen,"Performance of Space-Time Coded Transmitter Diversity Techniques in Transmission Scenarios of HiperLAN/2,," in *Proc. International ITG/IEEE Workshop on Smart Antennas*, Günzburg, Germany, Mar. 2006.

[42] A. Abdi and M. Kaveh, "A space-time correlation model for multielement antenna systems in mobile fading channels," *IEEE J. Select. Areas Commun.*, vol. 20, no. 3, pp. 550–560, Apr. 2002.

[43] A. Abdi, J. A. Barger, and M. Kaveh, "A parametric model for the distribution of the angle of arrival and the associated correlation function and power spectrum at the mobile station," *IEEE Trans. Veh. Technol.*, vol. 51, no. 3, pp. 425–434, May 2002.